

Research article

The Role of Geospatial Technology and Landform Mapping for Volcanic Secondary Hazard Anticipation in Semeru Volcano, Indonesia

Syamsul Bachri^{1,*}, Osamu Murao², Muhammad Naufal Fathoni³, A Riyan Rahman Hakiki⁴

¹ Department of Geography, Universitas Negeri Malang, Jl. Semarang 5, Malang 65145, Indonesia; ² International Research Institute of Disaster Science (IRIDeS), Tohoku University, Sendai, Miyagi, 980-8572, Japan; ³ Department Science and Geographic Information System, Universitas Gadjah Mada, Bulaksumur, Yogyakarta 0274-6492599, Indonesia, ⁴ Department of Geography Education, Universitas Lambung Mangkurat, Jl. Brigjend H. Hasan Basri, Kalimantan Selatan, Indonesia.

*) Correspondence: syamsul.bachri.fis@um.ac.id

Citation:

Bachri, S., Murao, O., Fathoni, M. N., & Hakiki, A. R. R. (2025). The Role of Geospatial Technology and Landform Mapping for Volcanic Se-condary Hazard Anticipation, Case Study Semeru Volcano, Indonesia. Forum Geografi. 39(2), 163-187.

Article history:

Received: 23 April 2025 Revised: 22 July 2025 Accepted: 23 July 2025 Published: 30 July 2025

Abstract

The combination of geospatial technology and field-based evidence plays an important role and has become a fundamental information system for any disaster-related database, such as a map at the local and regional levels. This research aims to map the geomorphological conditions of the Semeru Volcano after the 2021 eruption and to identify the area of the rain-triggered lahar slide based on the geomorphological conditions. We used remote sensing, geographic information systems, and field surveys. Factors such as morphological condition, lava slide direction, granularity, and thickness were used to predict the secondary hazard zone. The results found that erosion and sedimentation processes of rain-triggered lahar materials dominated 32 landforms from the geomorphological analysis within the study area. The materials were massively distributed in the middle and low-depositional zones located in the Mandalika formation. The inverse distance weighted analysis of lahar materials showed that the distribution of lahar in the range of 0 - 18.5 m was piled up at the bottom of the deposition process. In addition, through granular analysis, fine materials were deposited at the lower zone as a continuous sedimentation process. The lahar direction analysis also shows that the lower zone is a dangerous slide zone with indications of many lava slides. This research proves that the combination of geospatial and field-based evidence can be used to predict the secondary volcano hazard.

Keywords: geospatial technology; landform mapping; secondary hazard; semeru volcano Indonesia; geomorphology.

1. Introduction

Mount Semeru, one of Indonesia's stratovolcano volcanoes, is 3776 meters above sea level and classified as an active volcano. It was developed by phreatomagmatic activity and frequent volcanic eruptions, as well as subduction from the development of the Eurasian and Indo-Australian Plates. (Solikhin *et al.*, 2012; Thouret *et al.*, 2007). According to (PVMBG, 2021), the massive eruption of mount Semeru occurred on December 4, 2021, as a result of the lava dome collapsing in response to intense rainfall. The eruption caused serious damage, with an eruption index/VEI scale of 3, and produced 3–15 km³ of pyroclastic debris.

During the eruption, there was an increase in volcanic activity and a series of eruptions until December 31, 2021. The damage during the eruption caused by primary hazards such as lava flows, ejection of pyroclastic material, gas, and hot clouds. Eruption material scorch the vegetation, while volcanic ash piles up land, changing the volcano's land cover into open land that is easily deposited (Fathoni *et al.*, 2021). However, the threats are continued due the material eruption deposited after the first phase of eruption. Deposited volcanic materials pose a new potential threat in the form of secondary hazards, specifically rain-triggered lahars.

Rain-triggered lahars represent a potential secondary hazard that could persist after the eruption. Because of its rough structure and low water-holding ability, the material created during the eruption process is discharged swiftly. The material is dispersed over the volcano's steep slopes and is subsequently carried by river flows during periods of intense rainfall when the lava flows with a powerful and destructive intensity (Bachri *et al.*, 2019; Gomez & Lavigne, 2010).

Rain-triggered lahars pose a severe threat and damage to land. Their impact is not only limited in areas close to volcanoes, but rain-triggered lahar can threaten areas far away through river bodies and the topographic pathways. Research on lahar distribution modeling has been conducted by Gomez *et al.* (2018), measured boulders deposit along one of the lahar flows on mount Semeru. The study revealed that the distribution is largely controlled by slope geometry and gradient conditions. However, beyond slope information, identifying lahar-prone area requires consideration of physiographics conditions, the availability of loose volcanic materials, and the dominant geomorphic processes in a given area (Hadmoko *et al.*, 2018). In response to these needs, a comprehensive geomorphology-based approach using watershed analysis should be introduced as a



Copyright: © 2025 by the authors. Submitted for possible open access publication under the terms and conditions of the Creative Commons Attribution (CC BY) license (https://creativecommons.org/licenses/by/4.0/).

preliminary step for identifying rain-triggered lahar hazards. Geomorphology encompasses a broad scope of study as it serves to represent, analyze, and visualize Earth's surface forms and the processes shaping them. In geomorphological studies, an area is typically examined through four main approaches: the morphological (slope condition), morpho chronological (bedrock/surface material), morphoprocess (dominant process on landscape), and morpho-arrangement (structural/stratigraphic configuration of how a landscape is formed) (Barsch et al., 2007; Pavlopoulos et al., 2009). Several studies use geomorphological information as a zoning unit for lahar disasters (Lavigne et al., 2016) and a controlling factor for lava flood inundation (Procter et al., 2021). As a detail of lithological information, researchers (Kassouk et al., 2014), have developed derivatives of the geomorphological conditions of Mount Semeru using GIS and remote sensing approaches. However, the geomorphological approach has mainly been used to describe the locations affected by rain-triggered lahars and has not yet been applied to predict future landform changes. In this case, the landform alterations are caused by the processes or mechanisms of rain-triggered lahars. Where landscape conditions can change massively due to eruption phenomena. As consequences, geomorphological information as basic data needs to be updated, especially in the area of origin by the volcanic process. Geographic Information System (GIS) is becoming a fundamental information system for any disaster-related database at the local and regional levels (Tomaszewski et al., 2020). It is considered the primary mapping tool for disaster risk reduction (Hart & Hearn, 2018; Waleed & Sajjad, 2023). In addition, remote sensing images are used for the interpretation of risk resources and can be implemented for effective pre-disaster mitigation measures (Kaku, 2019; Khodaverdizahraee et al., 2020). The analysis has become easier and more effective with current high-precision remote sensing data, especially high-precision satellite images (Kaku, 2019; Niu et al., 2018). The combination of GIS and remote sensing has drastically changed the concept of mapping and spatial interpretation of risk and resources.

Geospatial-based predictive models have been developed in various countries. For example, lahar modeling based on morphometric parameters has been applied to Fuego Volcano in Guatemala to map flow paths and hazard zones (Cando-Jácome & Martínez-Graña, 2019). In Indonesia, a combined approach using geomorphological and hydrological data has proven effective in mapping lahar vulnerability at Mount Merapi (Lee & Lee, 2015). Meanwhile, spatial clustering methods originally developed for urban studies can also be adapted to systematically analyze volcanic hazard distribution. However, the high rainfall intensity and complex local morphology in tropical regions require further model adjustments.

Therefore, this study is designed to address the research gap concerning the limited of studies that comprehensively integrate geospatial technologies and geomorphological approaches to predict secondary hazards of rain-triggered lahars following the eruption of Mount Semeru. Specifically, this research try to address research question how geomorphological mapping units be utilized to analyze rain-triggered lahar dynamics. This study emphasizes the use of geomorphological mapping in delineating spatial distribution, identifying accumulation zones, and tracing lahar flow paths, an approach that has not been widely explored in the context of tropical lahar dynamics phenomena. Thus, the findings of this study not only expand academic understanding of secondary lahar dynamics but also offer a concrete contribution to more proactive and spatially updated disaster risk management efforts.

2. Research Methods

2.1. Study Area

The study sites included numerous administrative regions surrounding the semeru volcano, including Supiturang Village in Pronojiwo District and Sumberwuluh Village in Candipuro District, Lumajang Regency. These places were impacted by the Semeru Volcano eruption in 2021. The study also revealed secondary dangers associated with rivers serving as the movement of lava material in the event of lahar flows. Hence, this research used Rejali watershed as the study area (Figure 1).

Administratively, the Rejali watershed located in East Java's Lumajang Regency, which is divided into three sub-districts: Pronojiwo, Candipuro, and Pasirian. The Rejali watershed is situated at 8°06′34.19" to 8°17′26.98" South Latitude and 112°55′22.82" to 113°07′35.38" East Longitude, according to astronomy. The upstream region stretches southeastward and flows into the Indian Ocean. It is situated on the Semeru Volcano. In the downstream watershed area, the topography consists of plains, and the height varies from -4 to 3659 mdpl. The east of the watershed has a high and mountainous center region made of impermeable breccia rock, whereas the west of the watershed has undulating plains. In addition, this arrangement acts as a barrier for the middle and upstream.

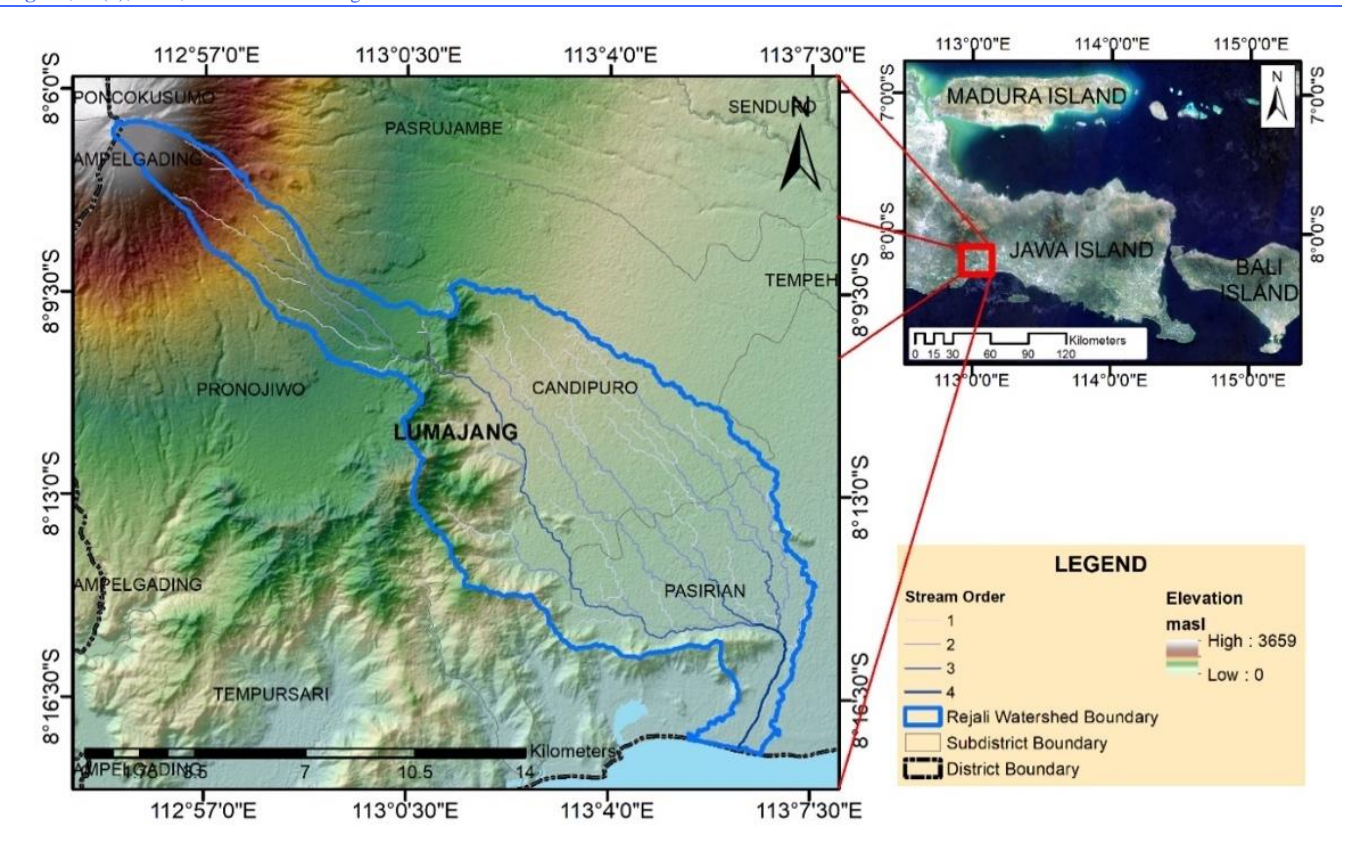


Figure 1. Study Area.

2.2. Data Collection

Data on rain-triggered lahar slides is displayed spatially as current lava conditions, and then possible slides are identified depending on field circumstances. These requirements led to the creation of two phases for the collection of research data: field surveys employing heuristics and geomorphology techniques, and remote sensing and geographic information system-based techniques.

2.2.1. Remote Sensing Data

By comparing past recordings to the temporal data acquired, remote sensing is able to determine regions affected by the lava slide. This data includes land dynamics. Relief extraction and geomorphology are two more analyses that make use of spatial topographical data in the form of a raster data model known as the Digital Elevation Model (DEM). Additionally, the application of DEM data in the field of numerical and static topographic analysis is expanded by the raster data model (distributed model) on altitude data in a number of studies (Boyong *et al.*, 2019; Jenson & Dominque, 1988), one of which is the prediction of rain-triggered lahar slide. Geological maps are another source of spatial information that can be used to ascertain the lithological conditions in the research area.

2.2.1.1. Sentinel-2 Data

Sentinel-2 Data, is optical remote sensing data that describes the condition of the land before and after the eruption. The condition of the land before the eruption was obtained from the recording on April 20, 2021, while the condition of the post-eruption land was obtained from the recording on April 5, 2022. Besides being used as an identification of the impact of the lava slide, the Sentinel-2 image after the eruption was also used for the identification of morphoprocesses and morpho-arrangements for the manufacture of geomorphological information. The product used is the Sentinel-2B Multispectral Instrument Image with a spatial resolution of 10 meters which was acquired temporally. The Level 2-A product was chosen as research data with geometrically corrected specifications and has a Bottom-of-Atmosphere (BoA) spectral correction level. Spectral correction in optical remote sensing images can improve display quality, especially when using 2 different recording images (Danoedoro, 2012).

2.2.1.2. National Digital Elevation Model Data

National Digital Elevation Model Data, is an Indonesian DEM product that has high spatial resolution. This data is classified as Digital Surface Model (DSM) data which still includes objects

above the ground such as vegetation and buildings. The National DEM was generated from a combination of several SAR datasets, including IFSAR data (5m resolution), TERRASAR-X (5m resolution), and ALOS PALSAR (11.25m resolution), supplemented with mass point data obtained through stereo-plotting. This processing resulted in a DEM with a spatial resolution of 0.27 arc-seconds or 8.1 meters, provided in GeoTIFF format with a brightness level of 32-bit float. In this study, DEM data is used without any filtering or conversion into Digital Terrain Model (DTM), considering that the research area consists of bareland—specifically, extensive lahar flow zones that are larger than the spatial resolution of the DEM. The DEM data were used for watershed extraction, classification of morphology and relief for geomorphological maps, and identification of flow accumulation.

2.2.1.3. Geological Map and Digital Earth Map of Indonesia

Lithological information was used as the basis for the creation of the geomorphological map, specifically in the form of morphochronological data. The geological map utilized was based on remote sensing image interpretation, produced by the Geological Survey Center of the Ministry of Energy and Mineral Resources (ESDM) in 2013. The maps used in the process of identifying geological materials in the Rejali Watershed area consisted of sheets with a scale of 1:50,000, including Ampelgading, Lumajang, and Tanjungan. The base map information was obtained from the Indonesian Digital Elevation Model Map at a 1:25,000 scale, provided by the National Geospatial Information Agency of Indonesia in 2021.

2.2.2. Geomorphological Approach-Based Field Survey

The field survey aimed to present an overview of actual field conditions, guided by a tentative hybrid map developed prior to fieldwork. This map was constructed by considering slope classifications, material types, and process identification, which were heuristically grouped through the interpretation of temporal imagery and validated by expert judgment. Additional information regarding the study area could be easily gathered during the field survey activities (Otto & Smith, 2013; Smith *et al.*, 2011). Another purpose of the field survey was to collect physical data on lahar material, validate and conduct ground-checking, and identify the impact of lahars on disaster-risk elements, both physical and other environmental components.

The field survey was conducted using purposive sampling based on the geomorphological units of the distal zone affected by lahars in the Rejali Watershed area. Geomorphological units were chosen as the unit of analysis because they represent the surface features and processes occurring within them, offering a useful framework for analysis and visualization. Geomorphological units classify the morphological features of the region, materials, and processes (time), and are widely used as analytical units in various studies related to lahar flow identification (Lavigne *et al.*, 2016; Pavlopoulos *et al.*, 2009; Procter *et al.*, 2021).

2.2.2.1. Ground Check and Updating Geomorphology Condition

Validation and ground-checking were carried out based on the previously created tentative geomorphological map to update the boundaries of land units. The identification of rain-triggered lahar impacts was conducted to assess the damage caused by the lahar flows. The identification activities carried out included: (a) morphological identification based on slope gradient information obtained through direct measurements using a distometer, (b) material identification, particularly in areas affected by rain-triggered lahars indicated by the presence of newly deposited materials, and (c) identification of the dominant geomorphic processes occurring in the field.

2.2.2.2. Identification of Existing Rain-Triggered Lahar Characteristics

As a key parameter related to lahar flow, the characteristics and properties of the lahar were identified in detail in the field. The field survey of lahar characteristics included: (a) identifying existing lahar flow paths using cross-sectional measurements at two affected locations, utilizing GPS plots and a distometer, (b) measuring lahar thickness using stratified random sampling at the research site, (c) qualitatively identifying and measuring the percentage of lahar material size in the field, and (d) collecting lahar deposit samples for sediment property and granulometric analysis through purposive sampling based on geomorphological units.

2.2.2.3. Identification of Rain-Triggered Lahar Impacts

Field observations also examined the extent of damage caused by the rain-triggered lahar flow. The impacts were categorized into: (a) effects on physiographic and geomorphological conditions, and (b) effects on exposed elements such as settlements, road access, plantations, and others. Observations were conducted by plotting the affected locations and qualitatively defining the resulting damage.

2.3. Data Processing and Analysis

2.3.1 Mapping the Geomorphological Condition of the Rejali Watershed

The geomorphological approach is a comprehensive classification of land units. In this study, the mapping of geomorphological land units was identified using spatial data, remote sensing, and validated through ground checks and field measurements. According to (Pavlopoulos *et al.*, 2009), geomorphology is an approach that classifies land based on four main categories: morphology obtained from DEM data and relief, morphochronology, derived from geological data, morphoarrangement and morphoprocesses, based on heuristic remote sensing interpretation. The geomorphological boundaries resulting from heuristic interpretation possess unique characteristics, with tangible boundaries in the form of relief. These boundaries are not the result of direct overlaying of several parameters, thereby producing representative data that is easy to use (Sartohadi *et al.*, 2014).

2.3.1.1. Morphological Condition Extraction

The analysis used to obtain morphological information includes the extraction of slope steepness and hillshade, which are spatial analyses using Digital Elevation Model (DEM) data, in accordance with the slope classification of Dessaunetes, 1977 (Desaunettes, 1977) as a slope classification system that is representative of actual field conditions (Table 1). The On-Screen Image Interpretation (OSII) digitization process, based on slope and hillshade extraction results, is used to generalize morphological conditions in order to obtain representative boundaries based on terrain relief.

Table 1. Slope Gradient Classes and Landform Types Based on Dessaunettes Classification, 1977.

Slope Gradient (%)	Elevation Difference (m)	Landform Type
0-2	<1	Plain
2-8	1-10	Undulating Plain
8-16	1-10	Rolling Plain
>16	1-10	Hummocky Plain
>16	10-50	Low Hills
>16	50-300	Hilly
>16	>300	Mountainous

2.3.1.2. Heuristic Visual Interpretation

All spatial information used to identify geomorphological units was interpreted visually using the On-Screen Image Interpretation (OSII) method. This method accommodates the geomorphological concept heuristically by integrating morphological data (slope gradient and hillshade), morpho-arrangement and morpho-process (satellite imagery), and morpho-chronology (lithological information based on geological maps). These data layers were analyzed simultaneously based on expert judgment in the field of geomorphology. Furthermore, manual digitization allows for the delineation of boundaries between land units based on topographic conditions that are easily recognizable in the field.

2.3.1.3. Re-interpretation and Updating of Geomorphological Boundaries

Information obtained from field validation conducted during the field survey stage was subsequently used to update the boundaries of geomorphological units. In addition, supplementary information collected during field data acquisition was also utilized to update the attributes of each geomorphological unit. The output of this stage is a draft of the final geomorphological map of the Rejali watershed area following the 2021 eruption of Mount Semeru.

2.3.2. Identification of Existing Lahar Condition

2.3.2.1. Mapping the Existing Slide Zone

The lahar flow zones in the Rejali Watershed area were spatially identified using temporal remote sensing data from Sentinel-2B, which acquired conditions before and after the Semeru eruption in 2021. The delineation of boundaries was carried out visually and digitally by observing changes in land cover around rivers and floodplains in the Rejali Watershed. The lahar flow zones identified through remote sensing provided tentative spatial information that was subsequently validated in the field. Cross-sectional profiles, derived from field measurements of the affected areas,

were used to correct the delineation of the lahar flow boundaries on the tentative map. This correction was necessary due to the time difference between image acquisition and the field survey.

2.3.2.2. Lahar Thickness Point Interpolation

The lahar thickness data obtained from the field survey consists of point data with reference coordinates. The requirement for thickness information in this study pertains to the thickness conditions across the entire affected area (distal zone) of the Rejali Watershed. Based on this need, spatial analysis through interpolation was performed to determine the thickness values at surrounding locations. Previous studies (Pasaribu *et al.*, 2012; Pramono, 2008) recommended the Inverse Distance Weighted (IDW) interpolation method due to its ability to provide good accuracy for topographic and sedimentation studies. This method assumes that each elevation point exerts a local influence that diminishes as the distance increases (Azpurua & dos Ramos, 2010). The equation 1 for IDW interpolation, as proposed by Azpurua & dos Ramos (2010), is as follows:

$$Z^* = \sum_{i=1}^{N} \omega_i Z_i \tag{1}$$

Where Z^* represents the estimated value (thickness), Z_i is the known elevation value at point i among N known points, and ω_i is the weight value determined by the following equation $\underline{2}$:

$$\omega_i = \frac{h_i^{-p}}{\sum_{i=0}^n h_i^{-p}} \tag{2}$$

where p is the power parameter that determines the influence of each point (this study uses a power value of 2), and h_j is the distance between the interpolated point and the known elevation point, which is calculated using the following equation $\underline{3}$:

$$h_i = \sqrt{(x - x_i)^2 + (y - y_i)^2} \tag{3}$$

where (x, y) are the coordinates of the point to be interpolated, and (x_i, y_i) are the coordinates of the known thickness location. A total of 196 thickness points obtained from field measurements (direct measurements, measurements of lahar-affected objects, and scaled field photographs) were used as input for the interpolation process to generate the distribution of eruptive material thickness across the entire study area. The interpolated data were then trimmed according to the lahar flow boundaries identified from the existing flow zone analysis.

2.3.2.3. Lahar granulometry

Granulometric analysis of lahars was conducted to determine the grain size distribution, processed statistically, and to reflect the properties of the lahar. Laboratory analysis was performed to obtain the texture size of lahar deposits from six lahar sediment samples collected during the field data gathering. A 100-gram sample was taken through splitting to reduce subjectivity in the samples used for sieving, which was performed using a series of sieves with the sizes presented in Table 2.

Table 2. Number and size of mesh.

Number (Mesh)	Particle size (ml)
1	10 2
1	18
3	35 0.5
6	0.25
14	0.106
27	70 0.053
40	0.038
Pa	nn 0.019

The weight of the sand in each sieve fraction was then converted into a PHI scale using the cumulative curve (Figure 2) for statistical calculations of the sediment. This stage was carried out to determine the sediment properties at each observation site, focusing on average grain size (mean), grain size uniformity (sortation), skewness of grain size distribution, and the kurtosis or peakedness of the grain size distribution. The weight line derived from the cumulative curve was used to identify the sediment transport mechanisms, which are classified into: (a) traction

(materials transported by rolling along the riverbed), (b) saltation (materials transported by bouncing along the riverbed), and (c) suspension (materials transported while floating in the water column above the riverbed).

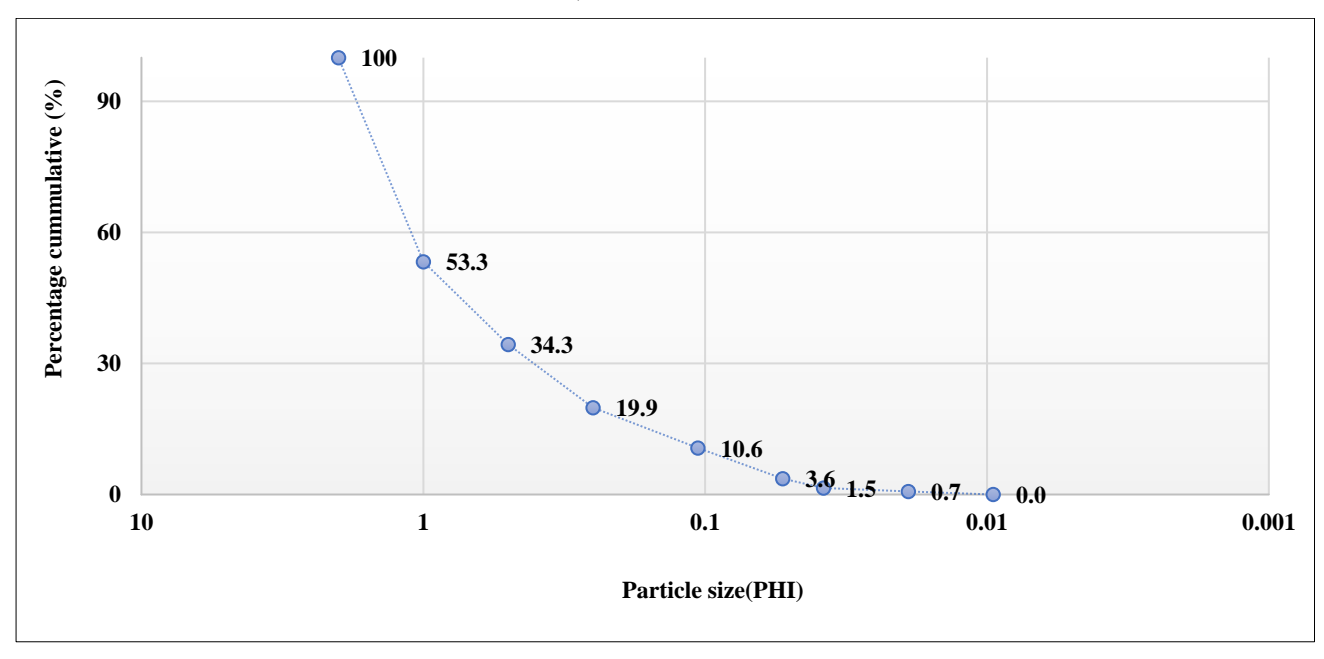


Figure 2. Example of a cumulative curve.

According the calculation of granulometric statistical parameters is based on the intersection between the cumulative curve and particle size (Φ) . The statistical parameter equations $\underline{4}$, $\underline{5}$, $\underline{6}$, & $\underline{7}$ used are as follows:

• Empirical Mean (Mean/Mz)

$$\frac{\Phi 16 + \Phi 50 + \Phi 84}{3} \tag{4}$$

Sorting Coefficient (Sorting/σ₁)

$$\frac{(\Phi 84 - \Phi 16)}{4} + \frac{(\Phi 95 - \Phi 5)}{6,6} \tag{5}$$

• Skewness (Skewness/Sk₁)

$$\frac{(\Phi 16 - \Phi 84 - 2\Phi 50)}{(\Phi 84 - \Phi 16)} + \frac{(\Phi 5 - \Phi 95 - 2\Phi 50)}{2(\Phi 95 - \Phi 5)} \tag{6}$$

• Kurtosis (Kurtosis/KG)

$$\frac{(\phi95 - \phi5)}{2,44(\phi75 - \phi25)}\tag{7}$$

2.3.3. Lahar Slide Prediction Based on Post-Eruption Existing Geomorphological Conditions

2.3.3.1. Updating DEM Data Based on the thickness of the lahar slide

The changes in geomorphology in this study focus on the topographic alterations caused by the covering of land by lahar flow material. The results of the lahar thickness interpolation from the previous identification stage were used as the topographic change values in the DEMNAS data. This was done using spatial analysis in the form of a raster mosaic with the "sum of values" option, resulting in a DEM with lahar thickness information.

2.3.3.2. Flow Accumulation as Glide Prediction

Flow accumulation is a raster-based spatial analysis that models the potential flow based on the accumulation/number of pixels influenced by surrounding pixels. The use of flow accumulation information in the modeling of lahar flows serves as the basis for determining the flow direction, as it is related to the identification of river channels as lahar transport pathways (Aisandy & Sukojo, 2016; Cando-Jácome & Martínez-Graña, 2019; Lee & Lee, 2015). The input data for this

analysis, in the form of DEM, is first extracted to provide flow direction information through spatial flow direction analysis. The flow concentration generated from each pixel will be directed toward a specific pixel and will accumulate as the number of contributing pixels increases. Figures 3 and 4 illustrate the schematic modeling of DEM data, flow direction, and flow accumulation.

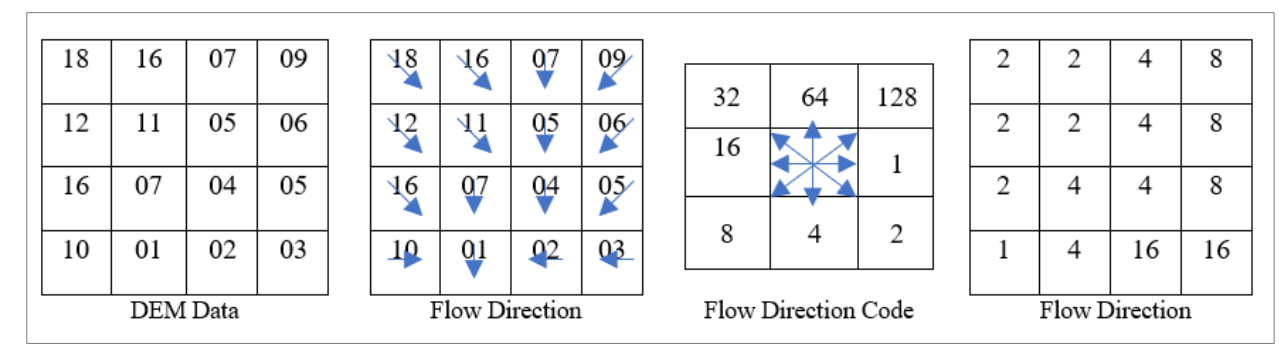


Figure 3. Sketch of DEM Data to Flow Direction.

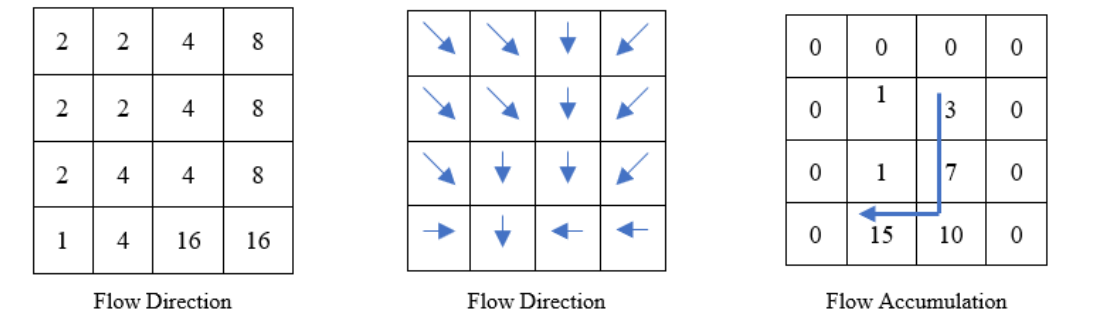


Figure 4. Sketch of Flow Direction to Flow Accumulation.

A higher flow accumulation value indicates that the location/pixel has a larger accumulation of flow. In relation to the research activities, the potential for lahar flows can be detected using the flow accumulation model, which directs the flow out of the identified existing lahar flow zone. The threshold value used for predicting lahar flows in this study is a flow accumulation value greater than 300.

3. Results and Discussion

3.1. Post-Eruption Existing Geomorphological Conditions

With a study analysis scale of 1:50,000, the geomorphological conditions of the Rejali watershed are displayed spatially. The data that is provided includes arrangements pertaining to the formation of a land, the dominant process, which is the identification of morphoprocess aspects, relief, which is the identification of morphology, and the origin of the process and surface material. Figure 5 displays the Rejali watershed's geomorphological condition map.

Based on the results of geomorphological map data processing (Figure 5), it was found that the Rejali Watershed had 32 landform units, which included landform units originating from volcanic, structural, fluvial, and marine processes. Landforms originating from volcanic processes dominated this area, with 23 landform units. Then, there were six fluvial landform units consisting of lahar floodplains flowing along the main river. Structural landforms were found in two areas in the form of the Mandalika formation and diorite rock intrusions. The structural landform formation had rock retention and structure that were not easily eroded by water, thus forming a bottleneck as a boundary between the upstream and central areas (Bachri, Fathoni, Masruroh, *et al.*, 2023). Marine-origin landforms were present in the downstream area, directly bordering the sea in the form of coastal alluvial plains.

The slope conditions were dominated by the formations of volcanic foot slopes in the central part of the watershed, undulating plains in the central to downstream parts of the watershed, and very steep slopes in the mountainous morphology. The plains morphology in the Rejali Watershed was dominant due to the watershed widening after entering the central area of the watershed. The smallest morphological unit was the valley formations in the mountainous morphology, which acted as a bottleneck separating the upstream and central areas of the watershed. The complete area of each morphological unit in the watershed is presented in Table 3.

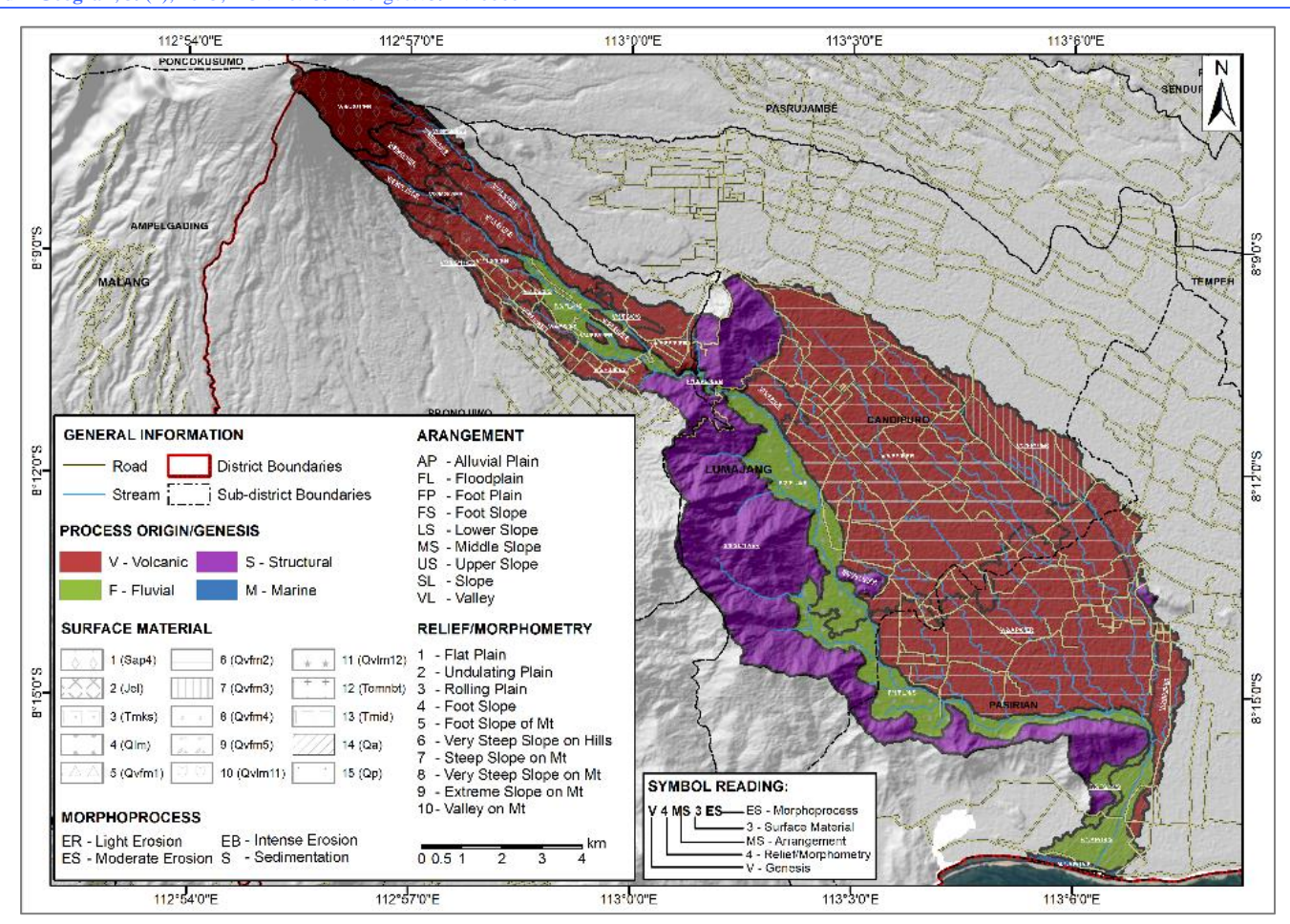


Figure 5. Geomorphological Map of the Rejali Watershed after the 2021 Semeru Volcano Eruption.

Table 3. The area of the Rejali watershed morphology class.

Morphological class	Area (Ha)
Flat Plain	931.45
Undulating Plain	3268.11
Rolling Plain	298.30
Foot Slope	74.24
Foot Slope on Mountain	4223.37
Very Steep Slope on Hills	53.63
Steep Slope on Mountains	803.63
Very Steep Slope on Mountains	3094.94
Extremely Steep Slope on Mountains	346.43
Valley on Mountains	23.13



Figure 6. Changes in river cliff morphology due to being covered by lahar material (right), remnants of river cliff collapse by lahars with large frequency and energy (left).

The differences in relief after the eruption in the Rejali Watershed area were caused by the erosion and sedimentation processes of lahar material, especially in areas adjacent to floodplains. Lahar material from the eruption, consisting of soil and rocks, was carried by water flow from the volcano slopes to the floodplains, resulting in significant changes in morphology and relief. Changes in geomorphological conditions (Figure 6) based on image analysis showed that the floodplains experienced an increase in area in the upstream region, which was then used as a new boundary indicator in the created geomorphological map.

Based on the results of lithological data processing, the Rejali Watershed had 15 lithological units, which are presented in Table $\underline{4}$.

Table 4. The geological formations of the study area.

Geology Formation	Symbol	
Jegung Lava Flow	Jel	
Alluvium Deposit	Qa	
Lahar Flow of Mount Mahameru	Qlm	
Alluvium and Beach Deposits	Qp	
Volcanic Lahar Fan Deposits Mt. Mahameru 1	Qvfm1	
Volcanic Lahar Fan Deposits Mt. Mahameru 2	Qvfm2	
Volcanic Lahar Fan Deposits Mt. Mahameru 3	Qvfm3	
Volcanic Lahar Fan Deposits Mt. Mahameru 4	Qvfm4	
Volcanic Lahar Fan Deposits Mt. Mahameru 5	Qvfm5	
Parasitic Lava Flow 11 Mt. Mahameru	Qvlm11	
Parasitic Lava Flow 12 Mt. Mahameru	Qvlm12	
Pyroclastic Flow Deposits 4 Mt. Mahameru	Sap4	
Breakthrough Rocks (Diorite and Porphyry)	Tmid	
Cylindrical Cone Deposits Totogan Malang	Tmks	
Breccia Tuff Mandalika Formation	Tomnbt	

The Rejali Watershed was classified as a dynamic area because it was located at the foot of Mount Semeru. This condition allowed for continuous land changes caused by primary and secondary volcanic hazards (Bachri *et al.*, 2021; Fathoni *et al.*, 2021).

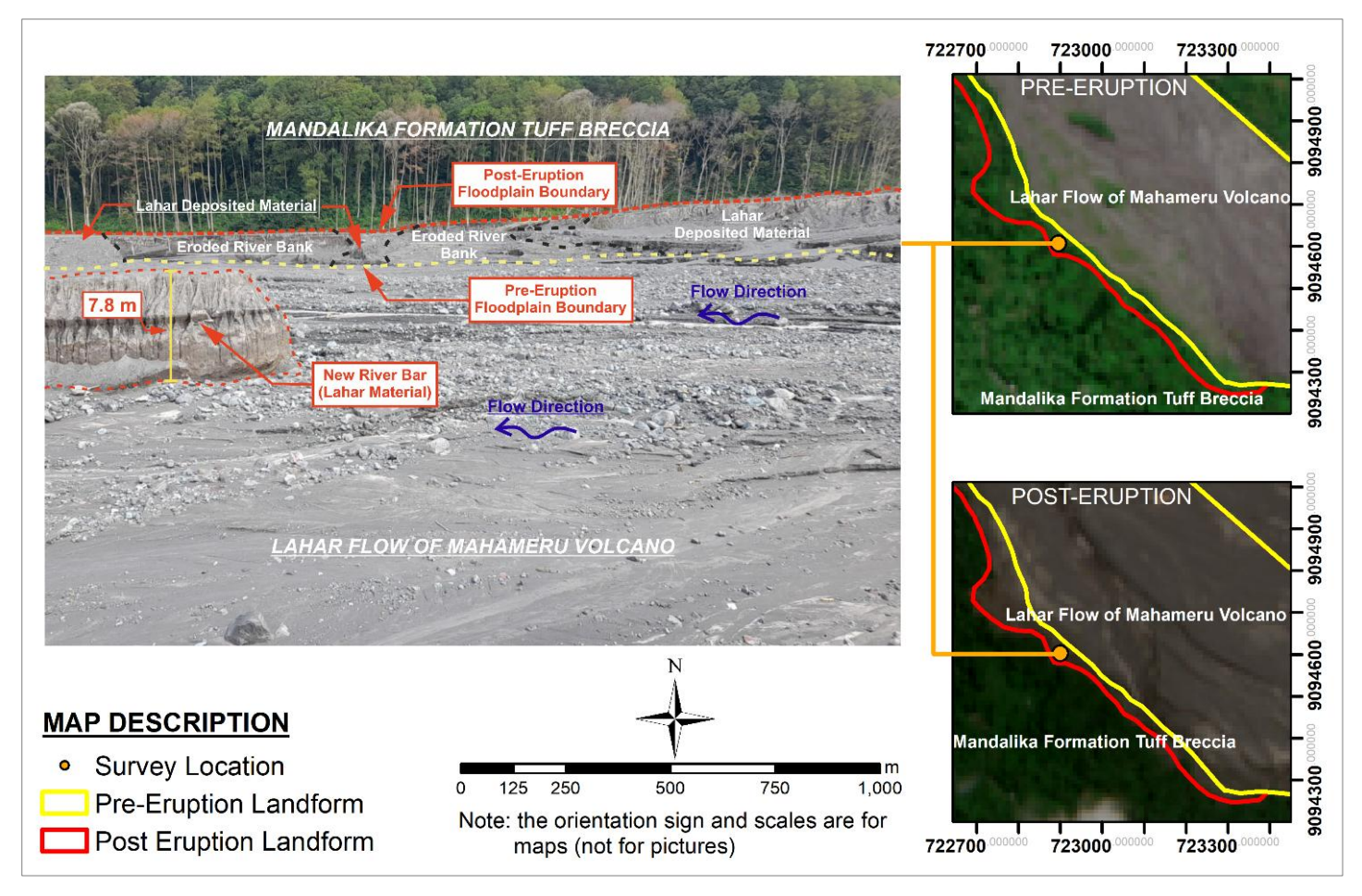


Figure 7. The identification of morphoprocesses, such as the expansion of lahar flow floodplains, using a remote sensing approach validated in the field.

The dominant changes that occurred in the Rejali Watershed were located in the upstream area and along the floodplain. In the upstream area, the predominant process was a high rate of erosion (Bronto, 2006; Munir *et al.*, 2024). This was caused by primary impacts in the proximal zone, such as the burning of land cover due to lava flows, pyroclastic flows, and the covering of land by pyroclastic material, which increased erosion (Idjuddin *et al.*, 2011; Sheets & Grayson, 1979). The dominant process along the floodplain was the morphological changes and the expansion of the lahar floodplain (Figure 7). This was due to the semi-fluid nature of lahar, whose energy and frequency could induce morphological changes in an area (Lavigne & Thouret, 2000). The overall aspects were identified heuristically, resulting in the naming and symbolization to facilitate information delivery. The naming and symbolization of landform units at the study area were presented in Table 5.

	Table 5. Symboliz	zation and N	aming of C	Geomorpholo	ogical Conditions.
--	--------------------------	--------------	------------	-------------	--------------------

No	Genesis	Symbol	Landform
1		V/10/US/1/EB	Upper Slope of Pyroclastic Flow Deposits 4 Mount Mahameru Heavily Eroded
2		V/9/MS/2/EB	Middle Slope Corn Lava Flow Heavily Eroded
3		V/9/MS/10/EB	Middle Slope Parasite Lava Flow 11 Mount Mahameru Severely Eroded
4		V/9/MS/1/EB	Middle Slope Pyroclastic Flow Deposits 4 Mount Mahameru Heavily Eroded
5		V/9/MS/1/ES	Middle Slope Pyroclastic Flow Deposits 4 Mount Mahameru Moderately Eroded
6		V/9/MS/3/ES	The Middle Slope of Malang Totogan Cylindrical Cone Deposits is Moderately Eroded
7		V/8/LS/11/EB	The Lower Slope of Parasite Lava Flow 12 Mahameru Mountain was Heavily Eroded
8		V/8/LS/1/EB	Lower Slope Pyroclastic Flow Deposits 4 Mount Mahameru Heavily Eroded
9		V/8/LS/1/ES	Lower Slope Pyroclastic Flow Deposits 4 Mount Mahameru Moderately Eroded
10		V/8/LS/9/EB	Lower Slope Volcanic Lava Fan Deposits 5 Mount Mahameru Heavily Eroded
11		V/8/LS/9/S	Lower Slope Volcanic Lava Fan Deposits 5 Sedimentary Mount Mahameru
12	Volcanic	V/5/FS/8/EB	Foot Slope of Volcanic Lava Fan Deposits 4 Mount Mahameru Heavily Eroded
13		V/5/FS/8/ER	Foot Slope Volcanic Lava Fan Deposits 4 Mount Mahameru Lightly Eroded
14		V/5/FS/8/S	Foot Slope Volcanic Lava Fan Deposits 4 Sedimentary Mount Mahameru
15		V/4/FS/9/EB	Foot Slope of Volcanic Lava Fan Deposits 5 Mount Mahameru Heavily Eroded
16		V/5/FS/9/ES	Foot Slope Volcanic Lava Fan Deposits 5 Mount Mahameru Lightly Eroded
17		V/4/FS/9/ES	Foot Slope Volcanic Lava Fan Deposits 5 Mount Mahameru Moderately Eroded
18		V/4/FS/9/S	Foot Slope Volcanic Lava Fan Deposits 5 Sedimented Mount Mahameru
19		V/5/FP/6/ER	Foot Plain of Volcanic Lava Fan Deposits 2 Mount Mahameru Lightly Eroded
20		V/5/FP/6/S	Foot Plains of Volcanic Lava Fan Deposits 2 Sedimented Mount Mahameru
21		V/5/FP/7/ER	Foot Plain of Volcanic Lava Fan Deposits 3 Mount Mahameru Lightly Eroded
22		V/2/AP/5/ER	Wavy Alluvial Plain Volcanic Lava Fan Deposits 1 Mount Mahameru Slightly Eroded
23		V/2/AP/6/ER	Wavy Alluvial Plain Volcanic Lava Fan Deposits 2 Mount Mahameru Slightly Eroded
24	Structural	S/9/SL/12/ER	Mandalika Formation Breccia and Tuff Slope Slightly Eroded
25	Structurar	S/7/SL/13/ER	Diorite and Porphyry Slopes Slightly Eroded
26		F/11/VL/4/EB	Mount Mahameru Lava Flow Valley Heavy Erosion
27		F/1/FL/4/S	Sedimentation of Mount Mahameru's Flood Plain Lava Flow
28	Fluvial	F/3/FL/4/S	Sedimentation of Wavy Flood Plain Lava Flow of Mount Mahameru
29	1 Iuviai	F/2/FL/4/S	Sedimentation of Wavy Flood Plain Lava Flow of Mount Mahameru
30		F/1/AP/14/S	Alluvial Plains Sedimentation
31		F/5/FS/14/S	Alluvial Deposits Foot Slope Sedimentation
32	Marine	M/1/AP/15/S	Fluviomarin Plains Sedimentation

3.2. The condition of the existing lahar flow post the eruption of Mount Semeru in 2021

3.2.1. Deposition zone affected by lahars

The distribution of lahar materials identified based on remote sensing observations and field surveys was categorized into two types: eroded zones and deposited/sedimented zones. Eroded zones are characterized by horizontal widening of riverbanks and increased depth of river valleys vertically due to the impact of lahar materials (Hadmoko *et al.*, 2018). These zones are marked by locations with higher elevations (riverbanks and bottoms with significant height differences) than the peak of the lahar flow, leading to erosion of riverbanks by lahar materials (Kurnianto, 2019). Sedimented/deposited zones represent areas covered by lahar materials, characterized by locations with lower elevations than the peak of the lahar flow (Kurniawan *et al.*, 2019; Masitoh *et al.*, 2019). Figure 8 illustrates the different types of impacts from rain-triggered lahars validated through field profiling.

Field profiling was also used as quality control for the identification results of lahar boundaries using remote sensing (Mutaqin *et al.*, 2022.). Based on the results of cross-section mapping of the lahar-affected areas at two locations, there was a difference in length/horizontal distance between field data collection and boundary delineation in the imagery (Table 6).

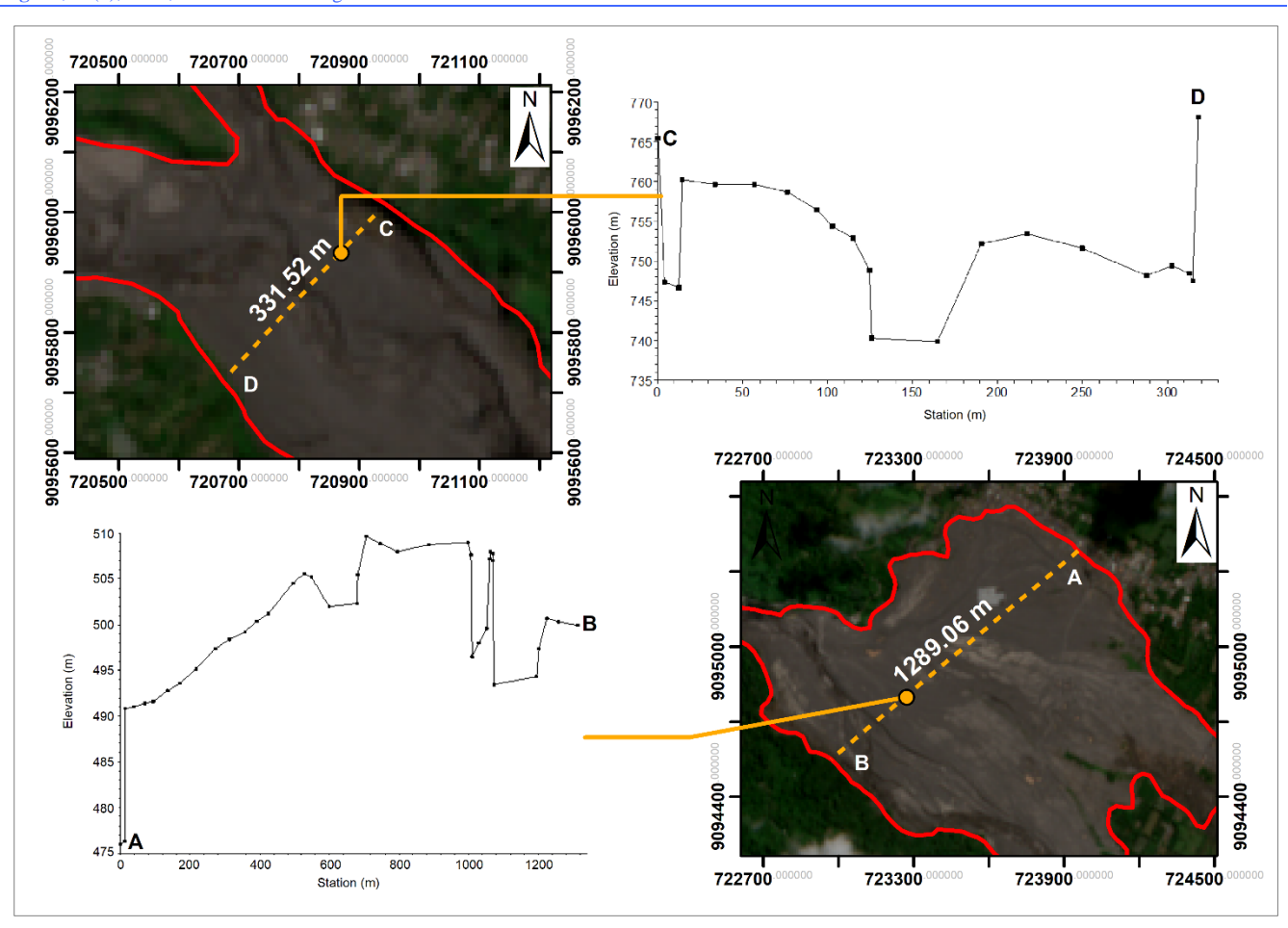


Figure 8. The zone of deposited/sedimented lahar materials (Profiling A-B) and the zone affected by lahar erosion (Profiling C-D).

Table 6. The difference in the lahar zone measurements was based on cross-sections and boundary delineation using remote sensing imagery.

Segment	Length in cross-section (m)	Imaging length (m)	Difference (m)
A-B	1313.6	1289.06	24.54
C-D	318.5	331.52	13.02
Mean diffe	rence		18.78

Based on the zoning identified using remote sensing, there was a difference in the area of lahar material distribution before and after the eruption, both in the erosion zone and the deposition zone. Based on area calculation of pre-eruption imagery, the lahar material in the pre-eruption condition was identified to cover an area of 1640.01 ha. Wheres, post-eruption imagery show that the distribution of lahar material increased to 2305.15 ha (40.56%) (Figure 9). Besides its temporal acquisition capability, remote sensing was able to identify areas that were inaccessible, such as steep slope regions (Joyce *et al.*, 2009; Rijal, 2020).

The distribution of the lahar deposition zone in the Rejali watershed, which had a massive impact, was located in the central area of the watershed, bordering the bottle neck formation of the Mandalika formation, characterized by the landform "Heavily Eroded Mahameru Volcano Lahar Valley". The Mandalika formation, with its retention properties and resistant rock structure, caused the concentration of lahar material transportation during peak discharge events (Widodo *et al.*, 2018). Additionally, another phenomenon that caused the lahar flow was the increasing perpendicular meanders of the river to the flow direction, leading to the lahar material diverting and overflowing from the river channel (Lestari *et al.*, 2019).

The distribution of the eroded lahar zone in the Rejali watershed, which had a massive impact, was located in the upstream area of the watershed before the bottle neck formation. The massive damage to the morphology included the erosion of the river bars with the landform unit "Heavily Eroded Foot Slope of Volcanic Lahar Fan Deposits 4 and 5 of Mount Mahameru" within the floodplain zone. This condition was caused by the accumulation of lahar material during peak discharge in the zone before passing through the bottle neck channel. The locations of the eroded and sedimented lahar material zones in the Rejali watershed are showed in Figure 2.

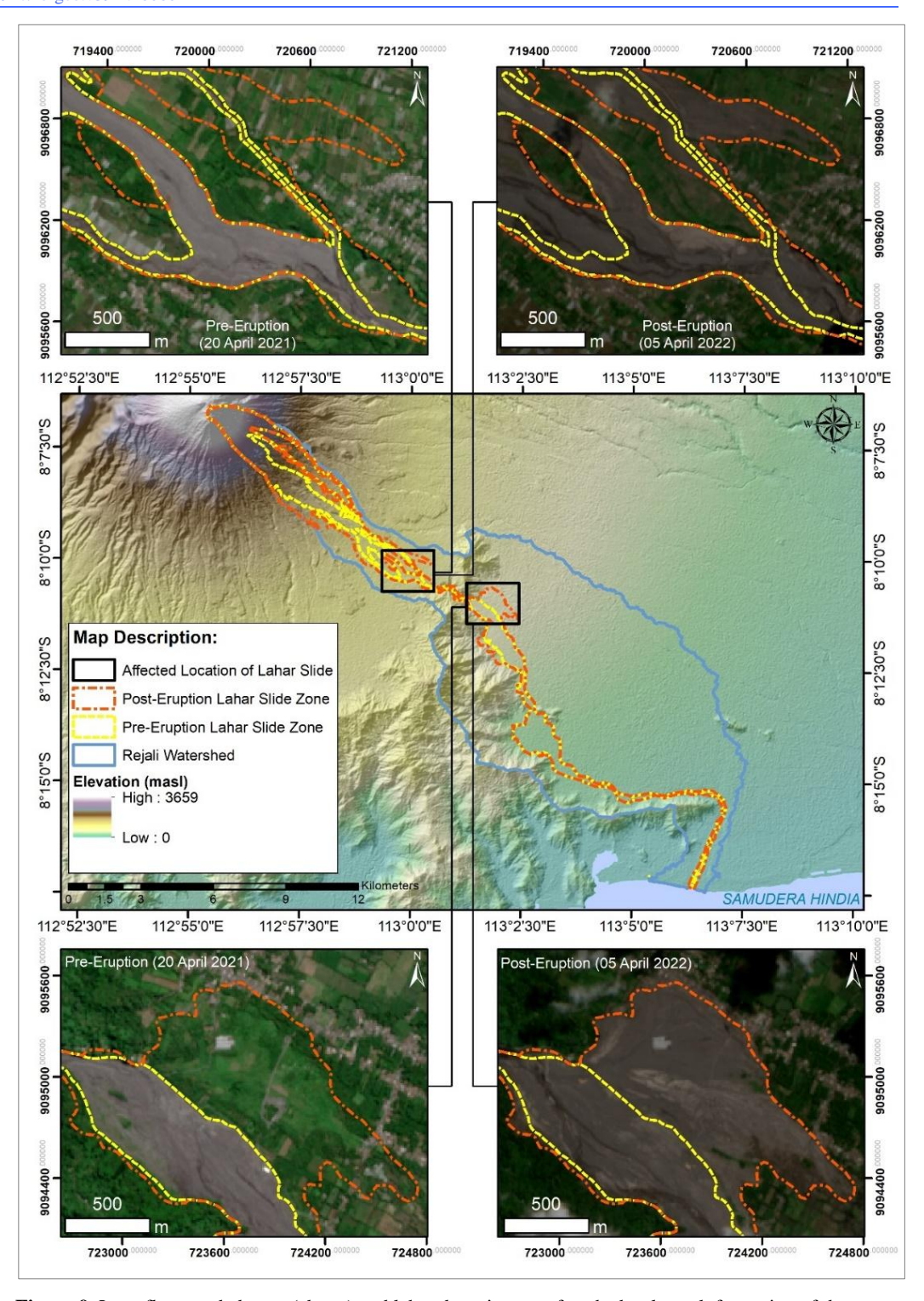


Figure 9. Lava flow eroded zone (above) and lahar deposit zone after the bottle neck formation of the mandalika formation (bottom).

The lahar-affected zone in the Rejali watershed predominantly occurred in areas with relatively gentle slopes, where the surface material consisted of previous lahar flow deposits. This phenomenon demonstrates that the processes occurring in a landscape at present are indicative of events that took place in the past (Cooke & Doornkamp, 1990; Hazbavi, 2018). In relation to disaster analysis, geomorphological landforms can be used as mapping units because they provide comprehensive information about a land area, including the dominant processes taking place.

3.2.2. Lahar Thickness Distribution

The identification of lahar material thickness in the field was observed using several methods, including direct measurement, estimation of affected objects, and profiling measurements (Figure 10). However, thickness information in the proximal zone, such as the upper and middle slopes of Mount Semeru, was not identified due to the difficult-to-access terrain conditions.



Figure 10. Field thickness measurement methods included direct measurement using a tape measure (left), esti-mation of affected objects (center), and profiling measurements using a distometer (right). Note: (a) lahar material deposits, (b) affected buildings, (c) lahar deposition.

There were 196 measurement points obtained in the field, with the maximum lava thickness reaching 18.5 meters and the minimum thickness being 0.1 meters. Based on all the measurement data, the average thickness in the Rejali Watershed flow zone reached 4.1 meters. The thickness mapping process was continued with interpolation to obtain the spatial distribution of thickness using spatial analysis in the form of digital interpolation (Adedapo & Zurqani, 2024; Akbarurrasyid & Kristiana, 2020; Ohashi & Torgo, 2012).

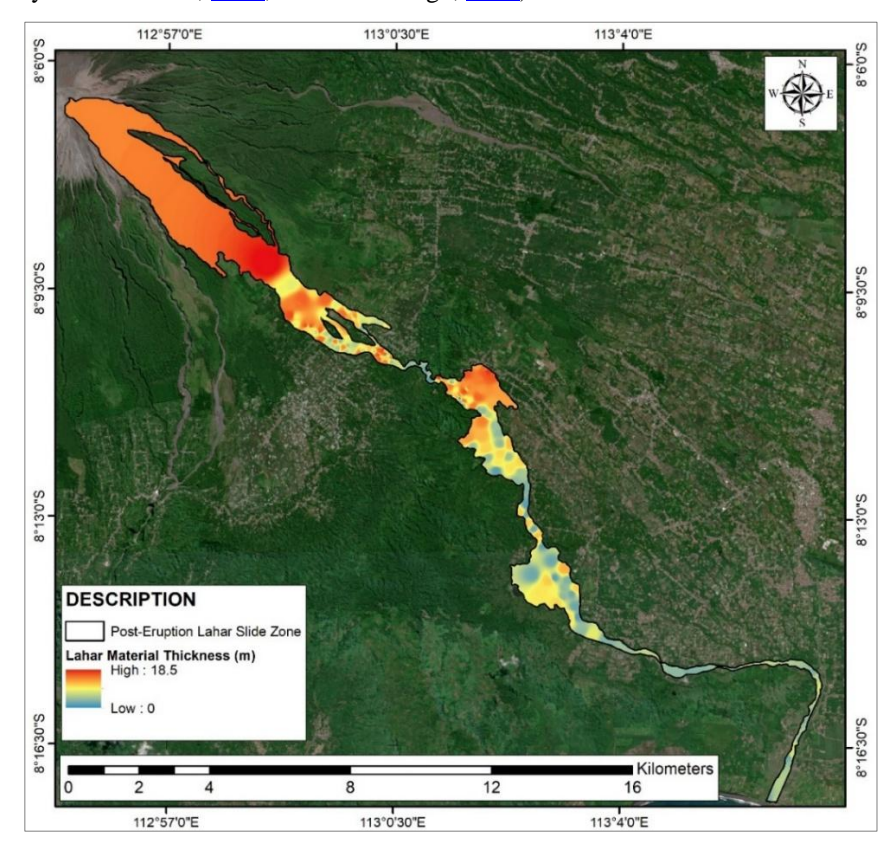


Figure 11. The thickness of the lava material in the slide zone after the eruption of the Semeru Volcano in the Rejali watershed area in 2021.

The Inverse Distance Weighted (IDW) interpolation method was used to produce the distribution of material thickness by considering the values between elevation points that decreased with increasing distance (Adedapo & Zurqani, 2024; Pasaribu & Haryani, 2012). The IDW method was widely used to model topographic conditions with measured points because it could accurately predict values between points. The spatial distribution of lahar material in the flow zone was presented in Figure 11.

The results of the IDW interpolation produced a distribution of lahar material thickness ranging from 0 to 18.5 meters. Material thickness less than 3 meters was located throughout the lower

middle zone to the downstream floodplain of the Rejali River, where flow energy began to decrease and carried little material. Lahar thickness less than 3 meters was also found in the bottle neck zone, which was the transition zone from the upstream to the downstream of the watershed. The minimal thickness of material in that zone was due to the watertight channel conditions, allowing all material to be carried to different zones. Material thickness between 3 - 12 meters was spread across the upper middle slope deposition area, bordering the bottle neck. This was caused by the concentration of material and energy that had passed through the narrow channel, resulting in a massive overflow phenomenon. Additionally, locations with similar thicknesses were sandbar areas eroded and buried by lahar material in the upstream region. Lahar material with thicknesses between 12 and 18 meters was identified at several points in the upstream area, marking the beginning of the distal zone. This condition was caused by a significant change in slope, leading to the deposition of lahar material before being carried to the lower zones.

3.2.3. Condition and Properties of Lahar

Six geomorphological unit locations were selected as observation zones, consisting of the upstream watershed area in unit (F/3/FL/4/S), bottle neck formation (F/11/VL/4/EB), middle watershed area (F/2/FL/4/S and F/1/FL/4/S), and downstream area (F/1/AP/14/S and M/1/AP/15/S). The qualitative observation results of lahar material were presented in Figure $\underline{12}$.

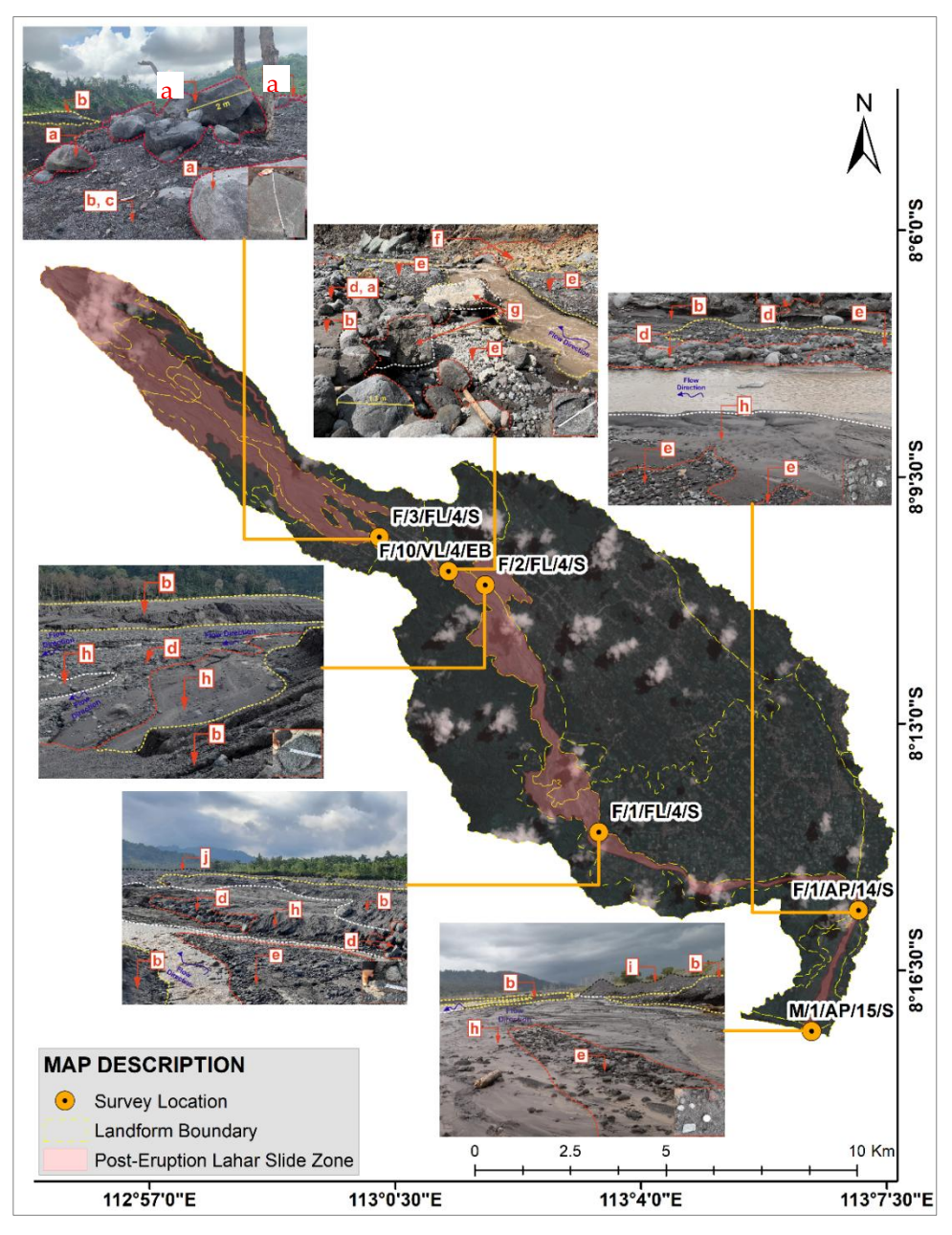


Figure 12. The location for observing lahar material used boundaries based on geomorphological landform units. Note: (a) boulders, (b) sands, (c) gravels, (d) cobbles, (e) pebbles, (f) riverbank ruins, (g) bridge collapse, (h) fine sand, (i) manual mining sand, (j) old deposits of cobbles and boulders.

The condition of lahar material in the "Wavy Floodplain Sedimentation of Mahameru Volcano Lahar Flow" zone (F/3/FL/4/S) was dominated sequentially by sandy material, gravel, pebbles, and bombs. This zone was a buildup of material before passing through the bottle neck formation. Bombs/large rocks with diameters greater than two meters were frequently found in this location, due to the landform being in the upstream area with wavy floodplain morphology, causing a reduction in flow energy. Additionally, the movement of bomb material was limited due to the bottle neck formation. Based on the condition and type of material size, zone F/3/FL/4/S had a relatively high hazard potential. This was because bomb-sized material had significant destructive power on geophysical aspects and human activity areas (Gomez & Lavigne, 2010).

The "Heavily Eroded Mahameru Volcano Lahar Flow Valley" zone /F/11/VL/4/EB, which formed the bottle neck, was sequentially dominated by lahar material such as pebbles, gravel, sand, and bombs. No sand material accumulation occurred at this location due to the concentrated flow that carried lighter materials and left larger and heavier materials like pebbles and bombs with diameters of 1-2 meters. It was classified as a landform with heavy erosion processes, as evidenced by the numerous landslide materials from the valley slopes (having a different color than the lahar material, which was Mandalika formation material) due to the high energy of the lahar flow. Based on the material conditions at location F/11/VL/4/EB, it had high destructive power due to the concentrated lahar flow in the bottle neck zone.

Zone F/2/FL/4/S or "Wavy Floodplain Sedimentation of Mahameru Volcano Lahar Flow" was a floodplain zone adjacent to the lahar deposition/flow zone. Located in the middle watershed area after the bottle neck formation, it caused sandy material to dominate and overflow into the surrounding area as a flow zone. Gravel and pebbles sized 20-60 cm were frequently found near the river flow, while bombs had a lower percentage. Fine sand material began to be found at this location due to the morphology, which was classified as an undulating plain. The dominant hazard potential at location F/2/FL/4/S was the massive overflow of sandy material in the surrounding floodplain area.

Zone F/1/FL/4/S or "Floodplain Sedimentation of Mahameru Volcano Lahar Flow" was a geomorphological unit similar to zone F/2/FL/4/S with a flat plain morphology. Located in the middle watershed area bordering the downstream area, the lahar material that dominated this area sequentially was sand and fine sand, gravel, pebbles, and bombs. The pebbles found were 15-30 cm in size with rounded and blunt shapes. Additionally, there were ancient bomb materials (not from the 2021 Semeru eruption lahar), marked by their rounded and blunt shapes, pushed by new lahar material and concentrated at the edge of the floodplain in several locations with flat morphology. The material shapes became more rounded and blunt downstream as the transportation distance increased (Dana *et al.*, 2016). Based on the type and size of material in zone F/1/FL/4/S, it had a low damage potential supported by the decreasing flow speed and lahar material transport speed due to the gentle slope conditions.

The landform zone F/1/AP/14/S or "Aluvial Deposit Plain Sedimentation" was a landform in the downstream Rejali Watershed area. The lahar material that dominated this location sequentially included sand, fine sand deposits, gravel, pebbles, and bombs. Fine sand deposits had a larger percentage than the landforms above due to the downstream morphology classified as a flat plain (Suriani *et al.*, 2024). Gravel and pebbles were frequently found in sizes of 5-20 cm mixed/bound by fine sand deposits. The damage potential from lahar material in this zone was low based on the identified material conditions.

Zone M/1/AP/15/S or "Fluviomarine Deposit Plain Sedimentation" was located at the river mouth directly bordering the sea. The morphology was classified as flat, with sedimentation as the dominant process due to wave flow opposing the river flow. The most common materials were fine sand deposits, sand, and gravel with diameters of 5-10 cm. Pebbles were found in small percentages, while bombs were not found at this location. Based on the material conditions and flow speed, the damage potential from lahar flow at this location was small. The identified lahar material widening in the image at location M/1/AP/15/S was not horizontal riverbank erosion but an increase in sediment material in the river body and floodplain.

As a complement to the qualitative description of lahar material properties, laboratory-based quantitative analysis was conducted to illustrate the variation in sediment grain size across zones representing the upper, middle, and lower parts of the study area. The upper zone, represented by F/3/FL/4/S, was dominated by medium sand-sized material (mean = 1.40 Φ), formed due to flow deceleration and intense material collisions before entering the bottleneck area. In the middle zone, represented by F/2/FL/4/S and F/1/FL/4/S, the average grain size was categorized as coarse sand (mean = 0.95–0.90 Φ). This condition indicates a mixture of saltation- and suspension-transported materials from the upper zone, with flat morphology enabling semi-fluid deposition.

Meanwhile, the lower zone, represented by F/1/AP/14/S and M/1/AP/15/S, was characterized by coarse to very coarse sand-sized material (mean = 0.23–0.21 Φ). The larger grain sizes in the lower zone resulted from sedimentation on flat terrain with low flow energy, along with the dominance of fine fractions such as very fine sand and silt.

3.2.4. Characteristics and Properties of Sediment Material

Granulometry analysis was used to measure the grain size of sediment to obtain its properties and characteristics quantitatively (Htun *et al.*, 2020a; Sayudi *et al.*, 2014). The material was described based on the mean grain size value to identify the grain size representing the entire sample (Boggs, 2012). Sortation was used to determine the uniformity of sediment grain size in rock sorting, with values obtained from standard deviation (Mir & Jeelani, 2015). The standard deviation value influenced the sorting value of a rock (Sasmito *et al.*, 2018). The larger the standard deviation obtained, the poorer the sorting of the rock, and vice versa.

The next parameter used was skewness, indicating the skewness level of a curve that described the coarseness/sharpness of the sediment material. Positive skewness indicated smooth-surfaced grains (Htun *et al.*, 2020b; P. S. Putra & Nugroho, 2017), while negative skewness indicated grains dominated by rough surfaces (Rozamuri & Hidayat, 2016). Kurtosis described the frequency distribution and grain size distribution in the analyzed sediment material. Kurtosis classifications included platycurtic, where sediment size distribution was evenly spread, mesokurtic, where sediment material was dominated, and lyptocurtic, where significant material dominance existed (Suriani *et al.*, 2024). The cumulative percentage curve from the granulometry analysis could also classify the sediment transport process into classes: traction (material rolling on the river surface), saltation (material deposited by hopping), and suspension (material carried by water currents). Granulometry analysis results were presented in Table 7, while cumulative percentage curves for each location were presented in Figure 13.

Location	Mean	Mean		Sorting		Skewness		Kurtosis		Precipitation Process	
Location	Value	Class	Value	Class	Value	Class	Value	Class	Traction	Saltation	Suspension
F/3/FL/4/S	1.40	MS	1.00	MdS	0	S	1.02	M	2%	13%	85%
F/11/VL/4/EB	0.85	CS	0.72	MdS	0.34	VF	0.28	VP	1%	26%	73%
F/2/FL/4/S	0.95	CS	0.72	MdS	0.37	VF	0.35	VP	5%	38%	57%
F/1/FL/4/S	0.90	CS	0.72	MdS	0.39	VF	0.28	VP	1.5%	47%	51.5%
F/1/AP/14/S	0.23	CS	0.20	VWS	0.58	VF	0.41	VP	3.5%	87.5%	9%
M/1/AP/15/S	0.21	CS	0.18	VWS	0.64	VF	0.53	VP	2%	92%	8%

Table 7. Results of granulometric measurements and laboratory sedimentation properties.

Legend: (a) mean = CS: coarse sand, MS: medium sand, (b) soriting = MdS: moderately sorted, VWS: very well sorted, (c) skewness = VF: very fine, S= symmetrical, (d) kurtosis = VP: very platykurtic, M: mesocurtic.

The sand at F/3/FL/4/S zone was categorized as medium sand with an average size of $1.40~\Phi$. This condition was caused by current speed (Rachman *et al.*, 2021) and intensive collisions between materials passing through the bottleneck, resulting in the accumulation of finer material. The mixing of materials in the upstream area indicated non-uniform material conditions, described by the moderately sorted sorting value. Intensive collisions between materials caused uneven material surfaces, seen from the symmetrical skewness value, and the dominance of material in a deposit was not uniform (mesocurtic). Based on the cumulative percentage curve, the dominant transport process in the F/3/FL/4/S landform was suspension (material dissolved by water), indicated by strong current speeds and high destructive power.

The sand deposits at F/11/VL/4/EB zone were categorized as coarse sand based on the obtained mean value of $0.85~\Phi$, consistent with field observations where the dominant material was coarse. The concentration of flow in the Mandalika formation valley area caused the material size to be not entirely uniform but evenly spread (platycurtic). The material surface was smooth due to erosion passing through the massive river walls. The material transport process was still dominated by suspension, where water discharge and current speed in the bottleneck zone were high.

Sand deposits at location F/2/FL/4/S were categorized as coarse-textured sand with a size of 0.95 Φ . The grain size was not entirely uniform but evenly spread (platykurtic) in the study location. The material surface was very smooth, giving it high sliding power. The dominant transport process was suspension, making the material semi-fluid and easily overflowing from the floodplain. The saltation process at location F/2/FL/4/S started to increase due to relatively flat slope conditions and reduced flow velocity. Material characteristics at zone F/1/FL/4/S were almost the same as the landform above it, F/2/FL/4/S. It had coarse sand texture material with a size of 0.90 Φ , not entirely uniform. The study location material was evenly spread with slightly rounded (smooth-

surfaced) material. This was due to the increasing saltation process, about 47%. However, the suspension process still dominated in the F/2/FL/4/S area, which was the middle part of the watershed area.

Landform F/1/AP/14/S was located in the downstream watershed area with a sloping plain. The material condition in this location was coarse-textured sand with uniform grain proportions. The deposit material properties were evenly spread in the observation area, characterized by smooth material surfaces. The dominant transport process in the downstream area was saltation due to the relatively calm and non-destructive river current (Gomez *et al.*, 2018b).

Lahar material conditions in the M/1/AP/15/S landform were categorized as coarse sand deposits with uniform grain size proportions evenly spread in the M/1/AP/15/S location. Characterized by very smooth grain surfaces with a dominant saltation process of 92%, lahar material damage was found in the downstream zone of the Rejali watershed due to very flat morphology conditions with low water flow energy.

The pattern of fine sediment accumulation identified in the downstream zone is not only caused by granulometric sorting processes but also by variations in slope gradient and flow velocity. The terrain slope gradually decreases (as indicated by the decreasing morphometric values in the geomorphological unit), particularly after passing through the bottleneck area of the Mandalika Formation. This slope reduction leads to a significant decrease in flow energy, thereby promoting the deposition of fine particles such as sand in flat areas. Gentle slopes below 8% are present in the downstream areas (for example, in land units F/1/AP/14/S and M/1/AP/15/S). Thus, the tendency for fine layering in the downstream zone is closely related to hydrodynamic deceleration and reduced transport capacity, reaffirming that slope gradient and flow energy are also key factors in the distribution of lahar sediments.

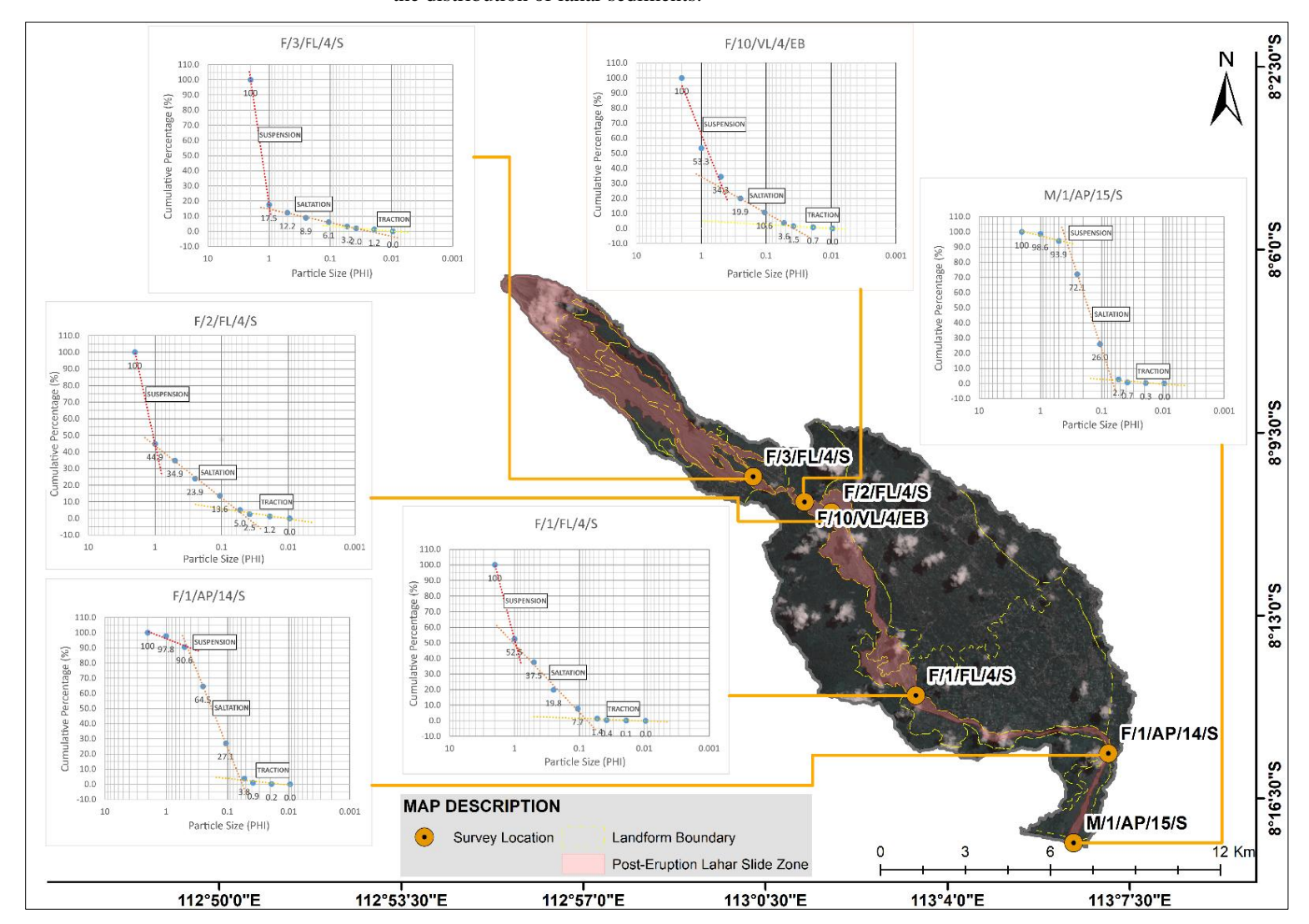


Figure 13. Cumulative percentage curve for the material distribution of the Semeru Volcano eruption in 2021.

3.2.5. Lahar Impact

Based on the characteristics of the rain-triggered lahar after the eruption of Mount Semeru in 2021, it provided an overview of the processes, mechanisms, properties, and spatial distribution of deposition zones. The rain-triggered lahar phenomenon that occurred in the Rejali watershed also intersected with human activities, causing losses (Anwar *et al.*, 2021). The encounter between the hazard phenomenon and vulnerability aspects resulted in losses of property, belongings, and lives, categorizing it as a disaster (Schneiderbauer *et al.*, 2017), in this case, the disaster being the flow of rain lahar. Several objects affected by the rain lahar disaster in the Rejali watershed, based on field data collection, could be categorized as damage to infrastructure, industry, and settlements.

The impact of rain-triggered lahar disaster damage on infrastructure in the Rejali watershed included the destruction of the Sabo Dam, which was used to restrain the lahar flow, and the disruption of transportation facilities such as roads and bridges. The Sabo Dam and the disrupted road network were located in the same area, namely Supit Urang Village, Pronojiwo District (Wahyuningtyas *et al.*, 2021). The condition of the damaged objects is showed in Figure 14.





Figure 14. Damage impact on the Sabo DAM (left) and the disruption of road access in Supiturang Village, Pro-nojiwo District, Lumajang Regency (right). Note: (a) Damage to the SABO DAM

The location of the Sabo DAM and the disrupted road network was situated in the upstream area of the Rejali watershed, bordered by a geomorphological bottleneck formation in the landform unit F/3/FL/4/S. The damage to the Sabo DAM was characterized by the destruction of the lahar material retaining embankment due to the concentration of lahar flow energy passing through the Mandalika rock formation valley. The damage to the highway access involved the disruption of the road crossing the floodplain of the Rejali River, which was one of the alternative routes connecting Malang Regency and Lumajang Regency (Thouret *et al.*, 2022).

The location that experienced massive lahar flow impacts was Sumberwuluh Village, Candipuro District, Lumajang Regency. The impacts included the disruption of the bridge transport network and the burial of settlements and industries in areas adjacent to the Rejali watershed floodplain (Bachri, *et al.*, 2023). The damage in Sumberwuluh Village is presented in Figure 15.

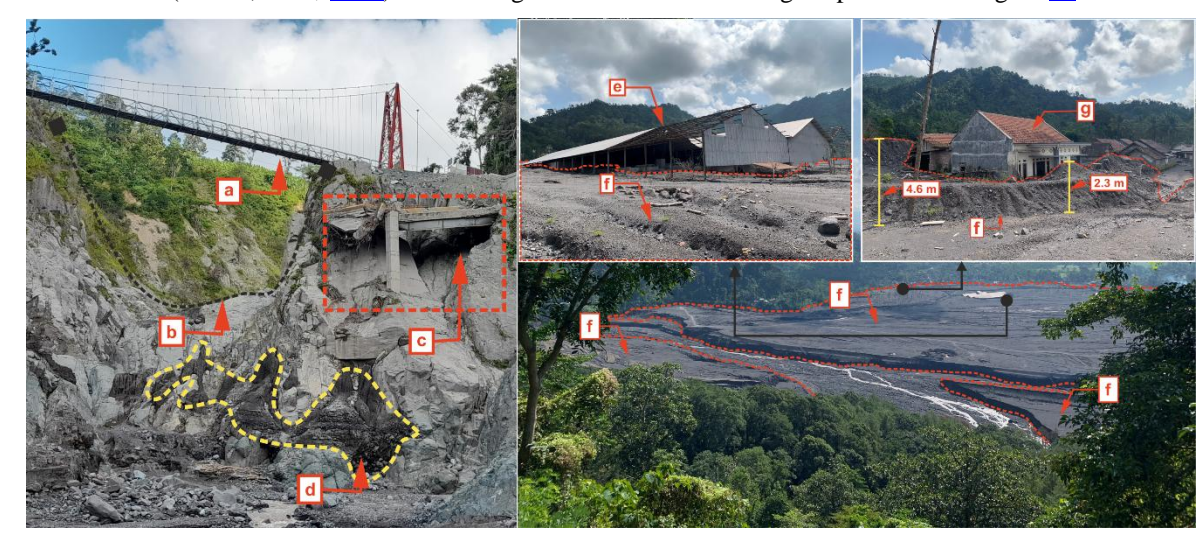


Figure 15. The condition of the damaged bridge (left) and the buried settlements and industries (right) in Sum-berwuluh Village, Candipuro District, Lumajang Regency. Note: (a) new bridge construction, (b) val-

ley of lahar flow landform, (c) affected bridge, (d) lahar sand material, (e) affected factory building, (f) lahar material, (g) affected buildings.

The high concentration of lahar in the upstream area was transported to the middle area of the watershed through the Lahar Flow Valley landform zone (F/11/VL/4/EB) with material characteristics of impermeable rocks. This location was the only channel connecting the upstream area to the middle area of the watershed, forming a bottleneck. During the peak discharge of lahar flow, the concentration of flow caused damage to the "Gladak Perak" bridge. This bridge was the main connecting route between Malang Regency and Lumajang Regency (Putra *et al.*, 2022).

The sandy material passing through the lahar flow valley zone had high energy and frequency, causing overflow in flatter zones located in the eastern part of the floodplain (landform unit V/5/FP/6/S). The impacts included the burial of settlements and industries with an average lahar material thickness of 6-8 meters. The impact of rain lahar in the middle to downstream areas of the watershed resulted in material deposits that did not cause damage. This condition was due to the low energy of the water flow, attributed to relatively flat relief and morphology classes.

Based on the thickness and grain characteristics of the lahar material collected in the field, it was found that the infrastructure damage zone, such as the sabo dam and bridge in Supiturang was buried under lahar deposits ranging from 5 to 10 meters in thickness. The dominant material in this area consists of large boulders (bombs) and coarse gravel, as identified in the landform units F/3/FL/4/S and F/11/VL/4/EB. Both zones are characterized by an average grain size ranging from coarse to very coarse sand (Φ 0.85–1.40) and a significant proportion of solid materials with diameters exceeding 1 meter. The combination of high material thickness and large grain size indicates a highly destructive energy, which led to structural failure of the dam and bridge.

3.3. Prediction of Lahar Flow Based on Geomorphological Conditions

Based on the existing conditions of rain-triggered lahar flows identified using remote sensing and field data collection, the next stage involved predicting lahar flows based on geomorphological information and lahar characteristics. The identified areas were distal zones, locations with secondary hazard potential from lahar flow.

Based on spatial analysis, information about geomorphological landform units before the eruption, which were impacted by lahar flows, was obtained (Table 8). This identification aimed to describe lahar flow locations and their potential based on a geomorphological approach. Landform units such as lahar flow floodplains and lahar flow valleys were not used as analysis units because these locations were natural zones for lahar material transport.

Landform	Area (ha)	(%)
Foot Plain of Volcanic Lava Fan Deposits 2 Mount Mahameru Lightly Eroded	98.2	31.8
Alluvial Plains Sedimentation	60.3	19.5
Foot Slope of Volcanic Lava Fan Deposits 5 Mount Mahameru Heavily Eroded	41.3	13.4
Mandalika Formation Breccia and Tuff Slope Slightly Eroded	33.6	10.9
Foot Slope Volcanic Lava Fan Deposits 4 Mount Mahameru Lightly Eroded	33.6	10.9
Foot Slope of Volcanic Lava Fan Deposits 4 Mount Mahameru Heavily Eroded	20.9	6.8
Foot Slope Volcanic Lava Fan Deposits 5 Mount Mahameru Lightly Eroded	8.4	2.7
Lower Slope Volcanic Lava Fan Deposits 4 Mount Mahameru Moderately Eroded	7.3	2.4
Foot Slope Volcanic Lava Fan Deposits 5 Mount Mahameru Moderately Eroded	3.1	1.0
Fluviomarin Plains Sedimentation	2.4	0.8

Table 8. Pre-Eruption Geomorphological Landform Units Affected by the Eruption.

Based on the results in Table $\underline{8}$, there were 10 geomorphological landform units before the eruption that were detected as zones impacted by lahar flows and experienced changes in both processes and morphological conditions. The highest impacted zone was 31.8% (98.2 ha) of the lahar flow zone in the distal area after the Semeru eruption, which was in the V/5/FP/6/ER zone or "Lightly Eroded Volcanic Lahar Fan Footplain of Mount Mahameru 2," located in the middle area of the watershed near the Mandalika formation bottleneck. The footplain had a slope of 0-8% and was associated with volcanic material. The V/5/FP/6/ER landform was also a meander formation after the Mandalika formation, resulting in the lahar flow easily overflowing during peak discharge. Based on a geomorphological approach, the V/5/FP/6/ER landform had the potential as a future lahar flow zone.

The landform unit V/5/FP/6/ER constitutes the area with the highest risk, as it is situated immediately downstream of the Mandalika bottleneck formation within a zone characterized by low slope gradients (<8%). These gentle slopes facilitate the dissipation of lahar flow energy, thereby promoting extensive sediment deposition. In contrast to the steeper upstream landforms that primarily function as conduits for energy transfer, the V/5/FP/6/ER unit acts as a terminal

accumulation zone that is highly susceptible to lahar overflows during peak discharge events. The reduced flow velocity in this area significantly increases the potential for lateral sediment expansion, posing direct threats to surrounding settlements, infrastructure, and agricultural land.

The results of the existing lahar characteristics survey, in the form of material thickness, were used to update the elevation data to identify new lahar flow zones. This was necessary because lahar material had low water-binding capacity, making it easily deposited (Arsyad, 2010; Idjuddin et al., 2011). The deposition of large amounts of material could potentially become a damaging lahar flow zone. Based on research (Arisandy & Sukojo, 2016), the flow potential extracted from elevation data could illustrate the direction of potential lahar flows validated with a disaster-prone area map. Higher flow accumulation values indicated that the area was a water channel serving as a lahar flow transport zone (Boyong et al., 2019; Cando-Jácome & Martínez-Graña, 2019). The spatial prediction of lahar flows in the V/5/FP/6/ER zone is presented in Figure 16.

The predicted lahar flow zone was symbolized by lines and arrow directions, providing information on the direction and reach of the flow. The direction information was obtained from flow accumulation lines starting from within the existing flow zone (symbolized in red) and heading outward to the V/5/FP/6/ER landform zone. The reach of the lines was determined by drawing the farthest boundary from the combined end arrowheads of the flow accumulation analysis, indicating the potential lahar flow distance.

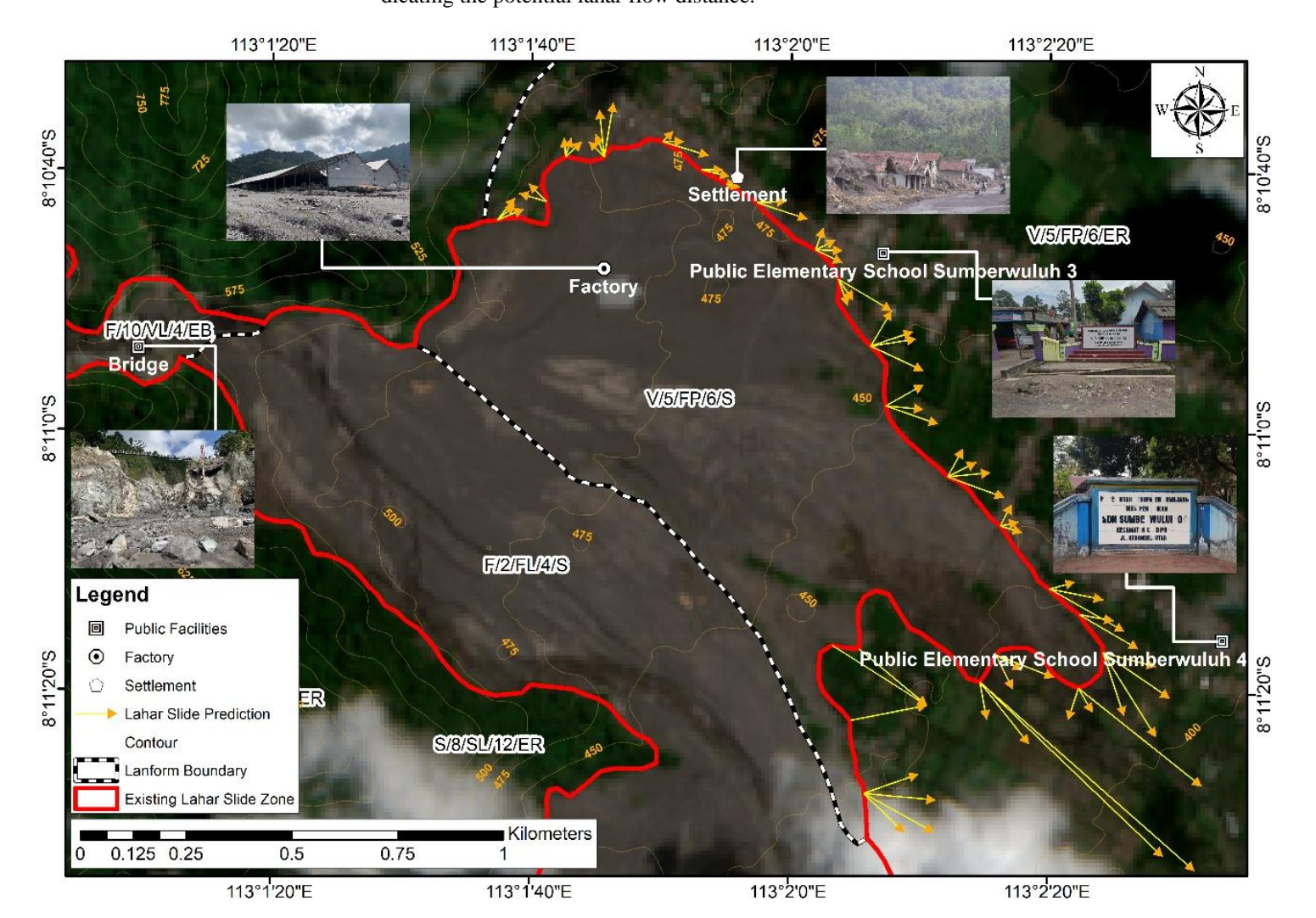


Figure 16. Lahar Flow Prediction Based on Geomorphological Approach and Flow Direction Accumulation.

Based on the lahar flow prediction zone, the spread of the flow direction extended outward from the existing flow zone, spreading into the V/5/FP/6/ER landform. Lahar material potentially deposited towards the southeast according to the slope direction, while on the eastern boundary of the existing lahar flow, the material had the potential to move northeast to southeast. The areas within the predicted lahar flow reach included agricultural areas to the southeast and several residential clusters and highways to the north and east. Other vulnerability aspects included two public facilities, namely elementary schools, located near the potential lahar flow.



Figure 17. Validation of Prediction Results through Field Survey.

To strengthen the results of the lahar flow path prediction based on geomorphological approaches and flow accumulation models, a field survey was conducted as a form of validation against real post-event conditions (Figure 17). This survey aimed to verify the alignment between the spatial modeling outputs and the actual distribution of lahar deposits in the field, as well as to identify directly affected risk elements. The findings from this validation indicate a strong correlation between the predicted lahar flow directions and the empirical conditions observed in the impacted locations, thereby reinforcing the reliability of the predictive model applied in this study.

4. Conclusion

This study highlights the vital role of integrating geospatial technologies and geomorphological analysis in anticipating the impact of rain-triggered lahars following the 2021 eruption of Mount Semeru. Through the combined use of remote sensing (Sentinel-2 imagery), high resolution digital elevation models (DEM), and field-based validation. The research successfully identified 32 geomorphological landform units within the Rejali Watershed that were significantly altered by secondary volcanic processes.

The findings reveal that lahar deposition and erosion processes were spatially concentrated in specific geomorphological zones, particularly in areas with varying slope gradients and lithological configurations. The bottleneck area formed by the Mandalika Formation served as a critical control point, where concentrated flow energy resulted in severe erosion upstream and massive sediment accumulation downstream.

Granulometric analysis of lahar deposits across representative upstream, midstream, and downstream zones further supported these spatial patterns. Sediment grain sizes exhibited a clear downstream fining trend, transitioning from medium sand in upper zones (F/3/FL/4/S), to coarse sand in midstream zones (F/2/FL/4/S and F/1/FL/4/S), and very coarse to fine sand in downstream zones (F/1/AP/14/S and M/1/AP/15/S). These patterns were closely linked to hydrological energy dissipation and topographic variation, which controlled the transport and deposition of volcanic material.

Furthermore, the study confirmed that certain geomorphological units, especially V/5/FP/6/ER, pose high risks due to their role as terminal accumulation zones in low-gradient terrain. These areas are particularly vulnerable to lahar overflows during peak discharge events, which can severely impact adjacent settlements, infrastructure, and agricultural land.

Ultimately, The results of the study demonstrate the potential of this method in assessing and predicting secondary hazards, particularly landform changes caused by rain-triggered lahars following the 2021 eruption of Mount Semeru. The findings serve not only academic advancement but also offer practical implications for disaster risk reduction, spatial planning, and community preparedness in volcanic regions.

Acknowledgements

The author is very grateful to Universitas Negeri Malang for supporting this research through the World Class University (WCU) Program. The first author also extends gratitude to the Government of Lumajang Regency, especially the Public Works and Spatial Planning Office of Lumajang Regency, and the Central Statistics Agency of Lumajang Regency for permitting and supporting research in the Mount Semeru area. Additionally, thanks to all institutions, parties, and teams that supported the completion of this research.

Author Contributions

Conceptualization: Bachri, S., & Murao, O.; methodology: Fathoni, M. N.; investigation: Hakiki, A. R. R.; writing—original draft preparation: Bachri, S.; writing—review and editing: Bachri, S.; visualization: Fathoni, M. N. All authors have read and agreed to the published version of the manuscript.

Conflict of interest

All authors declare that they have no conflicts of interest.

Data availability

Data is available upon Request.

Funding

This research received no external funding

References

- Adedapo, S. M., & Zurqani, H. A. (2024). Evaluating the performance of various interpolation techniques on digital elevation models highly dense forest vegetation environment. *Ecological Informatics*, 102646.
- Aisandy, A. S., & Sukojo, B. M. (2016). Studi Penentuan Aliran Hidrologi Metode Steepest Slope dan Lowest Height Dengan Aster GDEMV2 dan Alos Palsar (Studi Kasus: Gunung Kelud, Jawa Timur). *Jurnal Teknik ITS*, 5(2). doi: 10.12962/j23373539.v5i2.17162
- Akbarurrasyid, M., & Kristiana, I. (2020). Analisis Spasial Multi Kriteria untuk Menentukan Kesesuaian Lahan Tambak Budidaya Udang Vannamei (Litopenaeus vannamei): Biogeofisik dan Kualitas Tanah. Samakia: Jurnal Ilmu Perikanan, 11(2), 79–90.
- Anwar, N., Sofyan, A., & Jumaris, J. (2021). Kajian Kesiapsiagaan Masyarakat dalam Menghadapi Bencana Banjir Lahar Dingin di Kelurahan Tubo Kecamatan Ternate Utara Kota Ternate. *Pangea: Wahana Informasi Pengembangan Profesi Dan Ilmu Geografi*, 3(1), 181–188.
- Arisandy, A. S., & Sukojo, B. M. (2016). StudiPenentuanAliran HidrologiMetodeSteepest SlopedanLowest Heightdengan Aster GDEMV2 dan Alos Palsar (StudiKasus: Gunung Kelud, JawaTimur). *Jurnal Teknik ITS*, 5(2).
- Arsyad, S. (2010). Konservasi tanah dan air. IPB Press.
- Azpurua, M., & dos Ramos, K. (2010). A comparison of spatial interpolation methods for estimation of average electromagnetic field magnitude. *Progress In Electromagnetics Research M*, 14, 135–145. doi: 10.2528/PIERM10083103
- Bachri, S., Fathoni, M. N., Masruroh, H., Wibowo, N. A., Khusna, N., Billah, E. N., & Yudha, L. (2023). Geomorphological mapping and landform characterization of Semeru volcano after the eruption in 2021. IOP Conference Series: Earth and Environmental Science, 1180(1), 12004.
- Bachri, S., Fathoni, M. N., Sumarmi, Masruroh, H., Wibowo, N. A., Khusna, N., Billah, E. N., & Yudha, L. (2023). Geomorphological mapping and landform characterization of Semeru volcano after the eruption in 2021. IOP Conference Series: Earth and Environmental Science, 1180(1). doi: 10.1088/1755-1315/1180/1/012004
- Bachri, S., Irawan, L. Y., Wirawan, R., Nurjanah, A. E., Tyas, L. W. N., Utaya, S., & Sumarmi. (2019). Dynamics of Lahar Material Deposition Post 2014 Kelud Eruption of Bladak River. IOP Conference Series: Earth and Environmental Science, 256(1). doi: 10.1088/1755-1315/256/1/012021
- Bachri, S., Sumarmi, Irawan, L. Y., Fathoni, M. N., Fawaid, A. M., Nuraini, S. G., Utomo, K. S. B., & Aldianto, Y. E. (2021). Developing land capability to reduce land degradation and disaster incident in Bendo Watershed, Banyuwangi. IOP Conference Series: Earth and Environmental Science, 630, 012004. doi: 10.1088/1755-1315/630/1/012004
- Barsch, D., Fischer, K., & Stablein, G. (2007). Geomorphological Mapping of High Mountain Relief, Federal Republic of Germany. *Mountain Research and Development*, 7(4), 361. https://doi.org/10.2307/3673285
- Boggs, S. (2012). Principles of sedimentology and stratigraphy. Retrieved from https://www.academia.edu/dow-nload/112323865/9781292034515.pdf
- Boyong, S., Yogyakarta Verry Octa Kurniawan, D., Tyas Wulan Mei, E., & Sri Hadmoko, D. (2019). Pemodelan aliran lahar Gunung Api Merapi untuk perhitungan risiko kerugian pada penggunaan lahan terdampak di bantaran, 3, 2.
- Bronto, S. (2006). Fasies gunung api dan aplikasinya. Indonesian Journal on Geoscience, 1(2), 59–71.
- Cando-Jácome, M., & Martínez-Graña, A. (2019). Determination of primary and secondary lahar flow paths of the Fuego Volcano (Guatemala) using morphometric parameters. *Remote Sensing*, 11(6). doi: 10.3390/rs11060727
- Cooke, R. U., & Doornkamp, J. C. (1990). Geomorphology in Environmental Managemen: A New Introduction. Clarendon Press
- Dana, C. D. P., Sudirman, M. R., Noviana, A., & Hidayat, R. (2016). Analisis Granulometri, Morfologi Butir, dan Batuan Asal pada Endapan Pasir-Kerakal di Sepanjang Aliran Sungai Progo, D.I. Yogyakarta. Seminar Nasional Kebumian Ke-9, 776–786.
- Danoedoro, P. (2012). Pengantar Penginderaan Jauh Digital. Andi Publisher.
- Desaunettes, J. R. (1977). Catalogue of landforms for Indonesia: examples of a physiographic approach to land evaluation for agricultural development: prepared for the Land Capability Appraisal Project at the Soil Research. Institute. Bogor. Indonesia.
- Fathoni, M. N., Wicaksono, P., & Bachri, S. (2021). Estimated change in the percentage of vegetation cover after the eruption of Mount Agung, Bali in 2017. Seventh Geoinformation Science Symposium, 12082, 316-326. doi: 10.1117/12.2617334
- Gomez, C., & Lavigne, F. (2010). Automated block detection in lahars through 3-bands spectral analysis of video images. Journal of Volcanology and Geothermal Research, 190(3–4), 379–384. doi: 10.1016/j.jvolgeores.2009.11.005
- Gomez, C., Lavigne, F., Sri Hadmoko, D., & Wassmer, P. (2018a). Insights into lahar deposition processes in the Curah Lengkong (Semeru Volcano, Indonesia) using photogrammetry-based geospatial analysis, near-surface geophysics and CFD modelling. *Journal of Volcanology and Geothermal Research*, 353, 102–113. doi: 10.1016/j.jvolgeores.2018.01.021
- Gomez, C., Lavigne, F., Sri Hadmoko, D., & Wassmer, P. (2018b). Insights into lahar deposition processes in the Curah Lengkong (Semeru Volcano, Indonesia) using photogrammetry-based geospatial analysis, near-surface geophysics and CFD modelling. *Journal of Volcanology and Geothermal Research*, 353, 102–113. doi: 10.1016/j.jvolgeores.2018.01.021
- Hadmoko, D. S., de Belizal, E., Mutaqin, B. W., Dipayana, G. A., Marfai, M. A., Lavigne, F., Sartohadi, J., Worosuprojo, S., Starheim, C. C. A., & Gomez, C. (2018). Post-eruptive lahars at Kali Putih following the 2010 eruption of Merapi volcano, Indonesia: occurrences and impacts. *Natural Hazards*, 94(1), 419–444. doi: 10.1007/s11069-018-3396-7
- Hart, A. B., & Hearn, G. J. (2018). Mapping geohazards in the watersheds above Leh, Ladakh: The use of publicly-available remote sensing to assist risk management. *International Journal of Disaster Risk Reduction*, 31, 789–798. doi: 10.1016/j.ijdrr.2018.07.021
- Hazbavi, Z. (2018). Importance of Geology and Geomorphology in Watershed Health Assessment. *The Journal "Agriculture and Forestry*," 64(4). doi: 10.17707/AgricultForest.64.4.27
- Htun, M. M., Surjono, S. S., & Setyowiyoto, J. (2020a). Granulometry analysis of Ngrayong sandstone, Tempuran Area, Rembang Zone, North East Java Basin. IOP Conference Series: Earth and Environmental Science, 451(1), 012082.

- Htun, M. M., Surjono, S. S., & Setyowiyoto, J. (2020b). Granulometry analysis of Ngrayong sandstone, Tempuran Area, Rembang Zone, North East Java Basin. IOP Conference Series: Earth and Environmental Science, 451(1), 012082.
- Idjuddin, A. A., Erfandi, D., Soelaeman, Y., Suwanda, M. H., & Suganda, H. (2010). *Rehabilitasi dan konservasi tanah pasca-erupsi Gunung Merapi*. Kajian Cepat Dampak Erupsi Gunung Merapi.
- Jenson, S. K., & Dominque, J. O. (1988). Extracting topographic structure from digital elevation data for geographic information system analysis. *Photogrammetric Engineering and Remote Sensing*, 54(11), 1593–1600.
- Joyce, K. E., Samsonov, S., Manville, V., Jongens, R., Graettinger, A., & Cronin, S. J. (2009). Remote sensing data types and techniques for lahar path detection: A case study at Mt Ruapehu, New Zealand. Remote Sensing of Environment, 113(8), 1778–1786. doi: 10.1016/j.rse.2009.04.001
- Kaku, K. (2019). Satellite remote sensing for disaster management support: A holistic and staged approach based on case studies in Sentinel Asia. *International Journal of Disaster Risk Reduction*, 33, 417–432. doi: 10.1016/j.ijdrr.2018.09.015
- Kassouk, Z., Thouret, J. C., Gupta, A., Solikhin, A., & Liew, S. C. (2014). Object-oriented classification of a high-spatial resolution SPOT5 image for mapping geology and landforms of active volcanoes: Semeru case study, Indonesia. *Geomorphology*, 221, 18–33. doi: 10.1016/j.geomorph.2014.04.022
- Khodaverdizahraee, N., Rastiveis, H., & Jouybari, A. (2020). Segment-by-segment comparison technique for earthquake-induced building damage map generation using satellite imagery. *International Journal of Disaster Risk Reduction*, 46, 101505. doi: 10.1016/j.ijdrr.2020.101505
- Kurnianto, F. A. (2019). Proses Geomorfologi dan Kaitannya dengan Tipologi Wilayah. Majalah Pembelajaran Geografi, 2(2), 131–147.
- Kurniawan, V. O., Mei, E. T. W., & Hadmoko, D. S. (2019). Pemodelan aliran lahar Gunung Api Merapi untuk perhitungan risiko kerugian pada penggunaan lahan terdampak di bantaran Sungai Boyong, Pakem, Sleman, DI Yogyakarta. Jurnal Geografi Lingkungan Tropik (Journal of Geography of Tropical Environments), 3(2), 3.
- Lavigne, F., & Thouret, J. C. (2000). Lahars: Deposits, origins, and behaviour. Bulletin de La Société Géologique de France, 171(5), 545–557. doi: 10.2113/171.5.545
- Lavigne, F., Thouret, J.-C., Hadmoko, D. S., & Sukatja, B. (2016). Lahars in Java: Initiations, Dynamics, Hazard Assessment And Deposition Processes. Forum Geografi, 21(1), 5–24. doi: 10.23917/forgeo.v21i1.1822
- Lee*, S., & Lee, C. (2015). Detection and Hazard Mapping of Lahar and Pyroclastic Flow at Mount Merapi in Indonesia using the LAHARZ Program. *Near-Surface Asia Pacific Conference, Waikoloa, Hawaii,* 7-10, 124–126. doi: 10.1190/nsapc2015-032
- Lestari, N. K. D. A., Trigunasih, N. M., Dibia, I. N., & Suyarto, R. (2019). Interpretasi Citra untuk Analisis Kapasitas Sungai Unda sebagai Tampungan Lahar Dingin Erupsi Gunung Agung Bali. *Jurnal Agroekoteknologi Tropika*, 8(2), 222–230.
- Masitoh, F., Rusydi, A. N., & Diki Pratama, I. (2019). Kajian hidrogeomorfologi pada DAS orde 0 (nol) di Dusun Brau Batu. *Jurnal Pendidikan Geografi*, 24(2), 73–84.
- Mir, R. A., & Jeelani, G. H. (2015). Textural characteristics of sediments and weathering in the Jhelum River basin located in Kashmir Valley, western Himalaya. *Journal of the Geological Society of India*, 86, 445–458.
- Munir, M. D., Santoso, F. I., Eka, N. A., & Amanda, A. E. (2024). Lahar flow characteristic of Semeru Volcano based on Flow-R Model and its countermeasure. *IOP Conference Series: Earth and Environmental Science*, 1343(1), 012032
- Mutaqin, B. W., Amanatulloh, D. A., Waskita, T. B., Marfai, M. A., Isnain, M. N., Alwi, M., & Khomarudin, M. R. (2022). Analisis Geomorfologi dan Oseanografi untuk Identifikasi Tipologi Pulau Kecil: Studi Kasus di Kepulauan Maluku Utara dan Karimunjawa. *JPG (Jurnal Pendidikan Geografi)*, 9(1).
- Niu, X., Tang, H., & Wu, L. (2018). Satellite scheduling of large areal tasks for rapid response to natural disaster using a multi-objective genetic algorithm. *International Journal of Disaster Risk Reduction*, 28, 813–825. doi: 10.1016/j.ijdrr.2018.02.013
- Ohashi, O., & Torgo, L. (2012). Spatial interpolation using multiple regression. 2012 IEEE 12th International Conference on Data Mining, 1044–1049.
- Otto, J.-C., & Smith, M. J. (2013). Geomorphological mapping Field Mapping. *British Society for Geomorphology*, 6, 1–10.
- Pasaribu, J. M., & Haryani, N. S. (2012). Perbandingan teknik interpolasi DEM SRTM dengan metode Inverse Distance Weighted (IDW), natural neighbor dan spline (Comparison of DEM SRTM interpolation techniques using Inverse Distance Weighted (IDW), natural neighbor and spline method). *Jurnal Penginderaan Jauh Dan Pengolahan Data Citra Digital*, 9(2).
- Pasaribu, J. M., Suryo, N., Pemanfaatan, H. P., & Jauh, P. (2012). Perbandingan Teknik Interpolasi Dem Srtm Dengan Metode Inverse Distance Weighted (Idw), Natural Neighbor dan Spline (Comparison Of Dem Srtm Interpolation Techniques Using Inverse Distance Weighted (Idw), Natural Neighbor And Spline Method). Jurnal Penginderaan Jauh, 9, 2.
- Pavlopoulos, K., Evelpidou, N., & Vassilopoulos, A. (2009). *Mapping Geomorphological Environments*. Springer Berlin Heidelberg. doi: 10.1007/978-3-642-01950-0
- Pramono, G. H. (2008). Accuracy of the IDW and kriging methods for interpolating the suspended sediment distribution in Maros, South Sulawesi. *Forum Geografi*, 22(1), 145158.
- Procter, J., Zernack, A., Mead, S., Morgan, M., & Cronin, S. (2021). A review of lahars; past deposits, historic events and present-day simulations from Mt. Ruapehu and Mt. Taranaki, New Zealand. *New Zealand Journal of Geology and Geophysics*, 64(2–3), 479–503. doi: 10.1080/00288306.2020.1824999
- Putra, D. R. K., Kurniawan, L., Maarif, S., & Widodo, P. (2022). The Role of Lumajang's Regional Disaster Management Agency Facing of Semeru Volcanic Eruptions. *International Journal of Innovative Science and Research Technology*, 7(12), 1320–1325.
- Putra, P. S., & Nugroho, S. H. (2017). Distribusi Sedimen Permukaan Dasar Laut Perairan Sumba, Nusa Tenggara Timur. *OLDI (Oseanologi Dan Limnologi Di Indonesia)*, 2(3), 49–63.
- PVMBG. (2021). Press Release Aktivitas Vulkanik G. Semeru Jawa Timur 4 Desember 2021.
- Qurotulayun, A. A., Haribowo, R., & Sambah, A. B. (2023). The Impact of Mountain Semeru's Eruption on Groundwater Resources in the Rejali Watershed in 2021. *Jurnal Presipitasi: Media Komunikasi dan Pengembangan Teknik Lingkungan*, 20(2), 481-493.
- Rachman, R. A., Wibowo, M., Wiguna, E. A., Nugroho, S., Madyani, M., & Santoso, B. (2021). Kajian Karakteristik Sedimen Dasar di Perairan Sungailiat untuk Mendukung Pengembangan Pelabuhan Perikanan Nusantara Sungailiat, Kab. Bangka. *Buletin Oseanografi Marina*, 10(2), 112–122. doi: 10.14710/buloma.v10i2.31662

- Rijal, S. S. (2020). Identifikasi Material Piroklastik Pasca Erupsi Gunung Kelud Menggunakan Citra Hyperspektral (Hyperspectral Imagery for Identification of Kelud Volcano Pyroclastic Material). Jurnal Penginderaan Jauh Dan Pengolahan Data Citra Digital, 17(1), 1–9. doi: 10.30536/j.pjpdcd.2020.v17.a
- Rozamuri, M. F., & Hidayat, R. (2016). Studi Awal Granulometri Pada Sungai Mandeh dan Sungai Nyalo, Teluk Mandeh, Kabupaten Pesisir Selatan, Sumatera Barat. Seminar Nasional Kebumian Ke-9, 754–764.
- Sartohadi, J., Sianaturi, R. S., Ramadhana, W., Maritimo, F., Wacano, D., Munawaroh, Suryani, T., & Pratiwi, E. S. (2014). Bentang Sumberdaya Lahan Kawasan Gunungapi Ijen dan Sekiternya (Yogyakarta). Pustaka Pelajar.
- Sasmito, K., Rindawati, P. I., Pradana, S. A., & Andika, B. (2018). Analisis Lingkungan Pengendapan Dengan Metode Analisis Granulometri Daerah Tanah Merah Kota Samarinda, Kalimantan Timur. JURNAL TEKNIK GEOLOGI: Jurnal Ilmu Pengetahuan Dan Teknologi, 1(1).
- Sayudi, D. S., Wirakusumah, A. D., & Putra, R. (2014). Mekanisme pengendapan lahar sungai boyong di gunung merapi berdasarkan analisa granulometri. *Jurnal ESDM*, 6(1), 26–34.
- Schneiderbauer, S., Calliari, E., Hagenlocher, M., Bonadonna, C., Simmons, D. C., Simmons, D. C., Gowland, R., & King, A. G. (2017). Understanding disaster risk: risk assessment methodologies and examples. Science for disaster risk management, 38-130.
- Sheets, P. D., & Grayson, D. K. (1979). Volcanic Activity and Human Ecology.
- Smith, M. J., Paron, P., & Griffiths, J. S. (2011). GEOMORPHOLOGICAL MAPPING METHODS AND APPLICATIONS. Elsevier B.V.
- Solikhin, A., Thouret, J. C., Gupta, A., Harris, A. J. L., & Liew, S. C. (2012). Geology, tectonics, and the 2002-2003 eruption of the Semeru volcano, Indonesia: Interpreted from high-spatial resolution satellite imagery. *Geomorphology*, 138(1), 364–379. doi: 10.1016/j.geomorph.2011.10.001
- Suriani, P. D., Fajar, M. H. M., Ariyanti, N., Ramadhani, A. P., Ulumuddin, F., Rahayu, H. K., Wirayudhatama, M., Alfany, M. K., Rafi, M. E. D., & Zukhrufah, S. Z. (2024). Sediment Deposits Texture Analysis of Besuk Kobokan River in the Northern Slope Semeru Volcano Lumajang. *IOP Conference Series: Earth and Environmental Science*, 1307(1), 012025.
- Thouret, J. C., Lavigne, F., Suwa, H., Sukatja, B., & Surono. (2007). Volcanic hazards at Mount Semeru, East Java (Indonesia), with emphasis on lahars. *Bulletin of Volcanology*, 70(2), 221–244. doi: 10.1007/s00445-007-0133-6
- Thouret, J. C., Wavelet, E., Taillandier, M., Tjahjono, B., Jenkins, S. F., Azzaoui, N., & Santoni, O. (2022). Defining population socio-economic characteristics, hazard knowledge and risk perception: The adaptive capacity to persistent volcanic threats from Semeru, Indonesia. *International Journal of Disaster Risk Reduction*, 77. doi: 10.1016/j.ijdrr.2022.103064
- Tomaszewski, B. M., Moore, E. A., Parnell, K., Leader, A. M., Armington, W. R., Aponte, O., Brooks, L., Herold, B. K., Meyers, B. S., Ruggero, T., Sutherby, Z., Wolters, M., Wu, S., Szarzynski, J., Greve, K., & Parody, R. (2020). Developing a geographic information capacity (GIC) profile for disaster risk management under United Nations framework commitments. *International Journal of Disaster Risk Reduction*, 47, 101638. doi: 10.1016/j.ijdrr.2020.101638
- Wahyuningtyas, N., Yaniafari, R. P., Rosyida, F., Megasari, R., Dewi, K., & Khotimah, K. (2021). Mapping a Eruption Disaster-Prone Area in The Bromo-Tengger-Semeru National Tourism Strategic (case study of Mount Semeru, Indonesia). *Geojournal of Tourism and Geosites*, 39(4), 1430–1438. doi: 10.30892/gtg.394spl14-787
- Waleed, M., & Sajjad, M. (2023). On the emergence of geospatial cloud-based platforms for disaster risk management: A global scientometric review of google earth engine applications. *International Journal of Disaster Risk Reduction*, 97, 104056. doi: 10.1016/j.ijdrr.2023.104056
- Widodo, A., Warnana, D. D., GNR, J. P., & Iswahyudi, A. (2018). Pemetaan Kerentanan Tsunami Kabupaten Lumajang Menggunakan Sistem Informasi Geografis. IPTEK Journal of Proceedings Series, 2.